

# RADIATION SHIELDING BY NATURAL TERRAIN ON THE SURFACE OF MARS

28<sup>th</sup> WRMISS Workshop  
September 4, 2025  
Cologne, Germany

Gabin Charpentier<sup>1,2,3</sup>, Bent Ehresmann<sup>4</sup>, Don Hassler<sup>4</sup>, Cary Zeitlin<sup>5</sup>,  
Robert Wimmer-Schweingruber<sup>6</sup>, Robert Ecoffet<sup>1</sup> and Yves Gourinat<sup>3</sup>

**[gabin.charpentier2@cnes.fr](mailto:gabin.charpentier2@cnes.fr)**

1 : Centre National d'Études Spatiales (CNES), Toulouse, France

2 : TRAD Tests & Radiations, Labège, France

3 : ISAE-SUPAERO, Université de Toulouse, Toulouse, France

4 : Solar System Science & Exploration Division, Southwest Research Institute (SwRI), Boulder, CO, USA

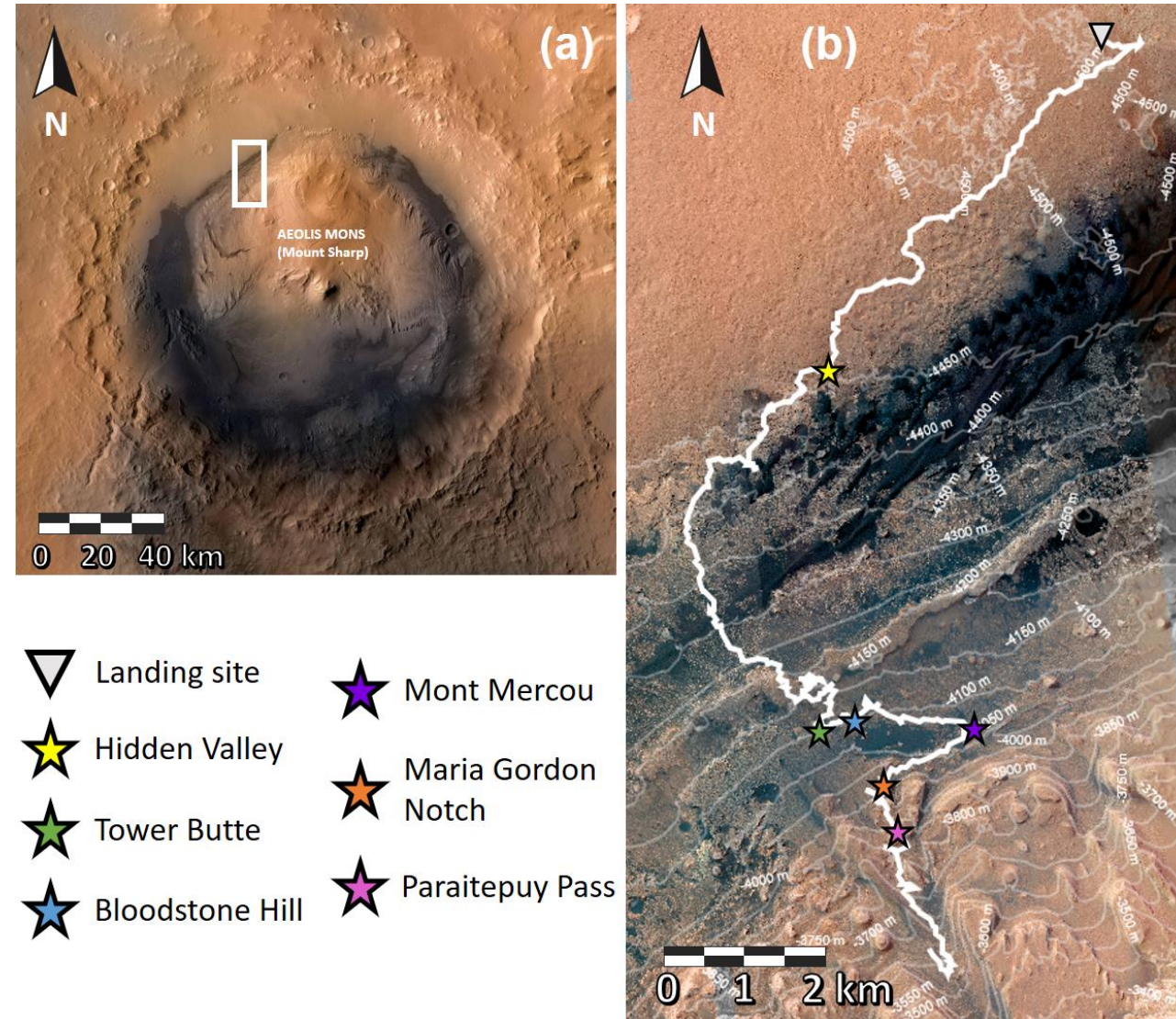
5 : Institute of Experimental and Applied Physics, Christian-Albrechts-University, Kiel, Germany



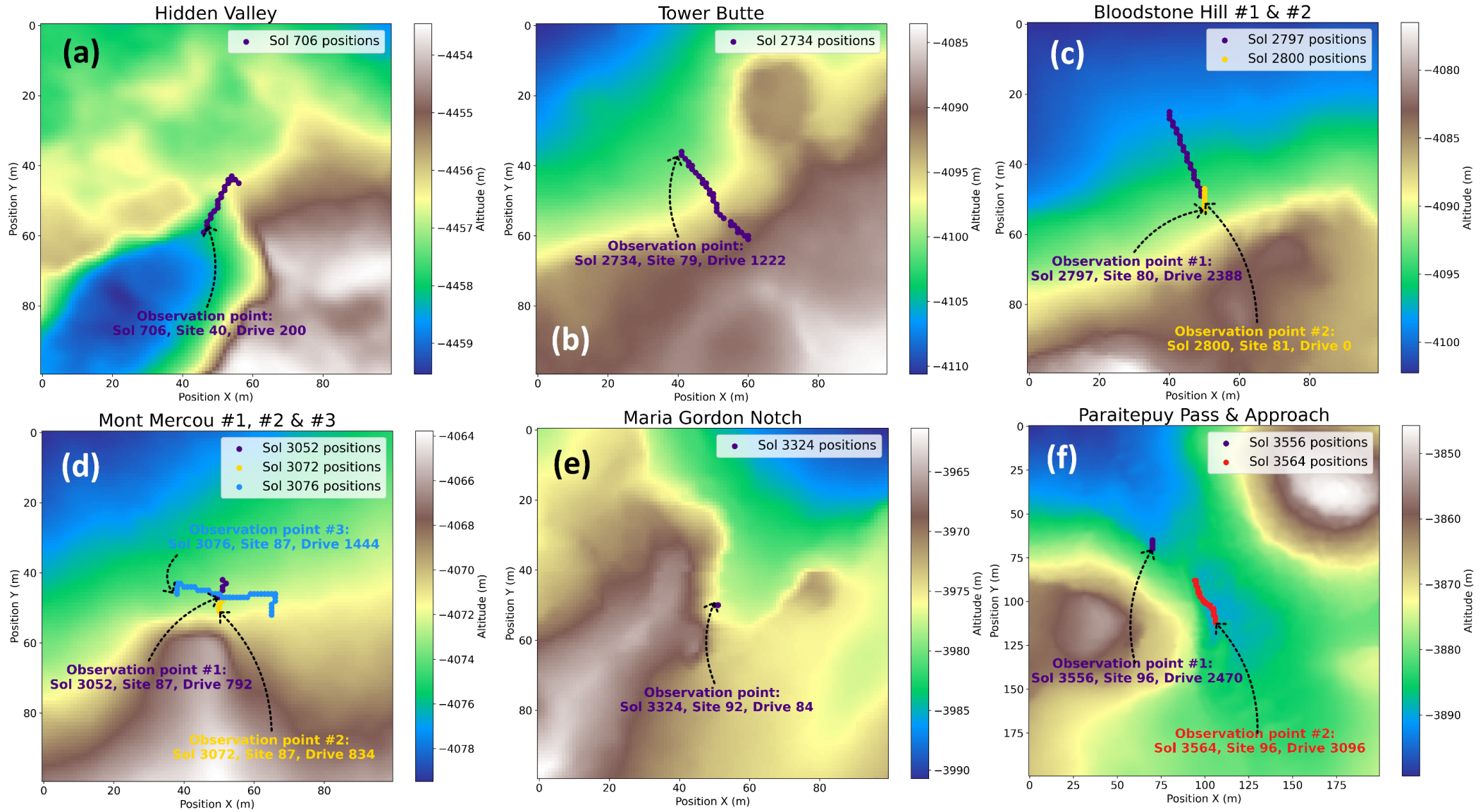
# Different sites of interest along MSL/RAD traverse path

- 6 sites of interest and in total 10 different points :

Location	Parking Sols	Rover Site/Drive
Hidden Valley	706-708	40/200
Tower Butte	2734-2742	79/1222
Bloodstone Hill - 1	2797-2800	80/2388
Bloodstone Hill - 2	2800-2802	81/0
Mont Mercou - 1	3052-3072	87/792
Mont Mercou - 2	3072-3074	87/834
Mont Mercou - 3	3076-3079	87/1444
Maria Gordon Notch	3324-3326	92/84
Paraitepuy Pass Approach	3556-3558	96/2470
Paraitepuy Pass	3564-3565	96/3096



# Different sites of interest along MSL/RAD traverse path

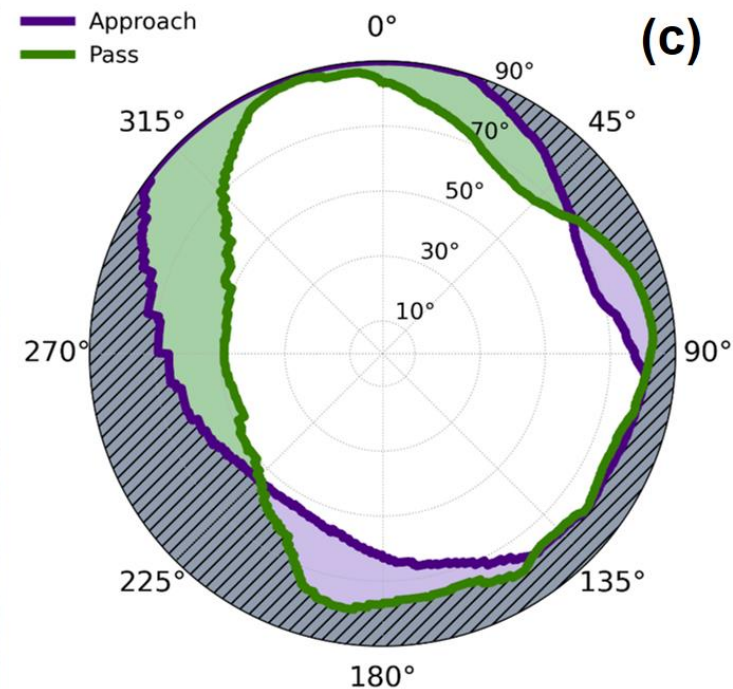
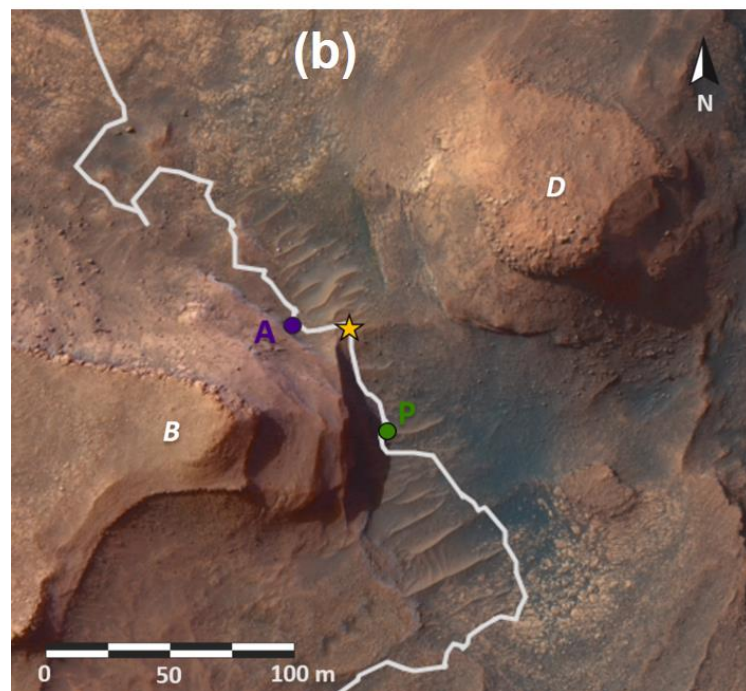
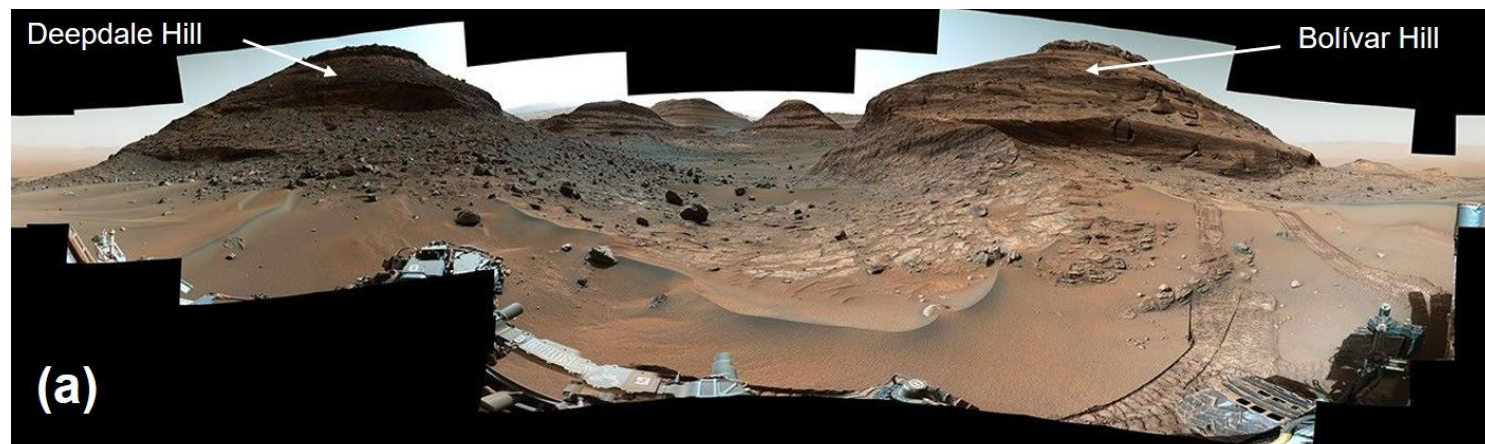


# The example of Paraitepuy Pass

- The horizon masks have been computed on the basis of a Digital Elevation Model (DEM) of the Gale Crater created by JPL/NASA/USGS/University of Arizona. This DEM has a resolution of 1m/pixel.
- The viewpoint was set up 1m above the surface to mimic RAD elevation, while the elevation angle of the horizon line was determined for azimuth angles intervals of  $0.25^\circ$  from 0 to  $360^\circ$ .
- For each azimuth angle the horizon elevation angle has been calculated using the horizon distance and planet curvature, within a radius of 20 km around the view point.

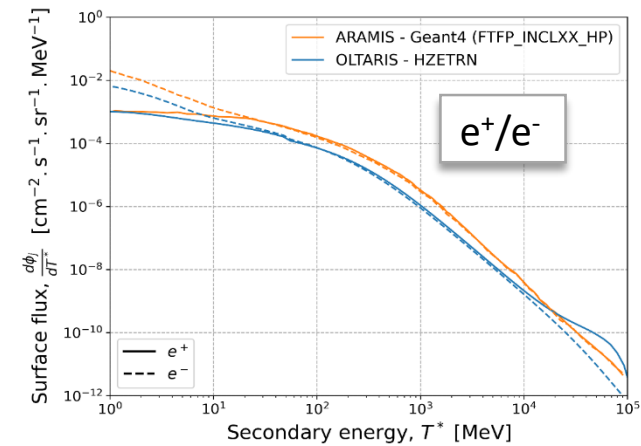
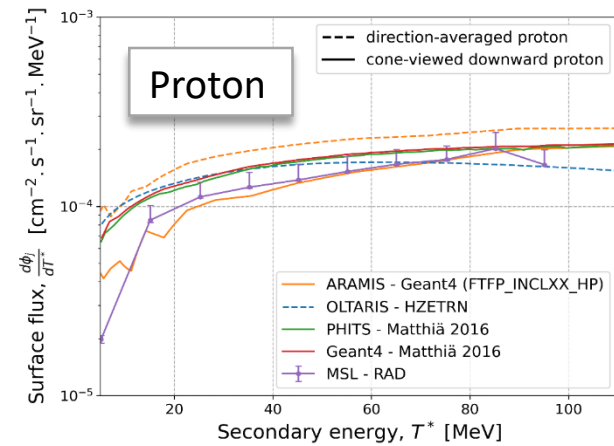
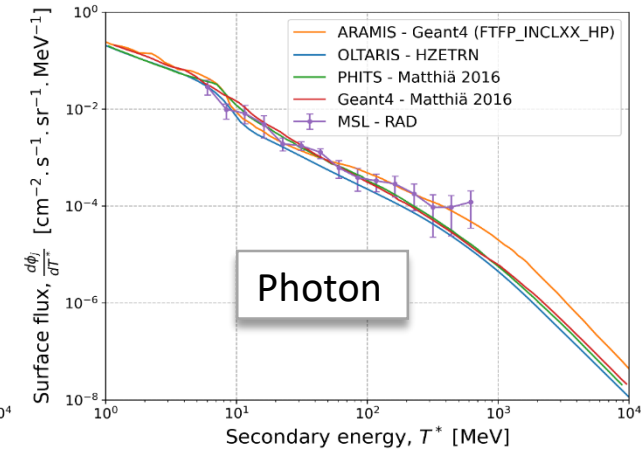
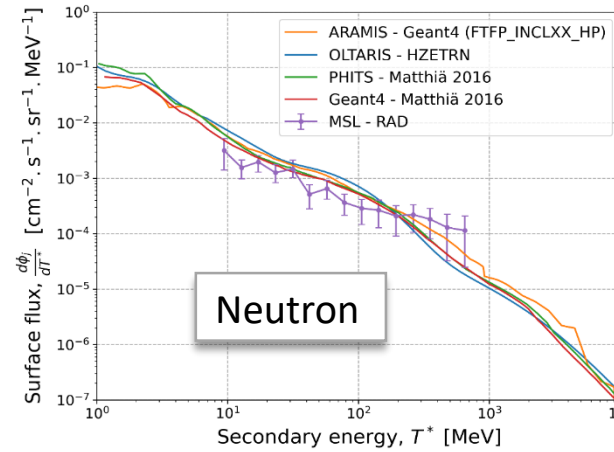
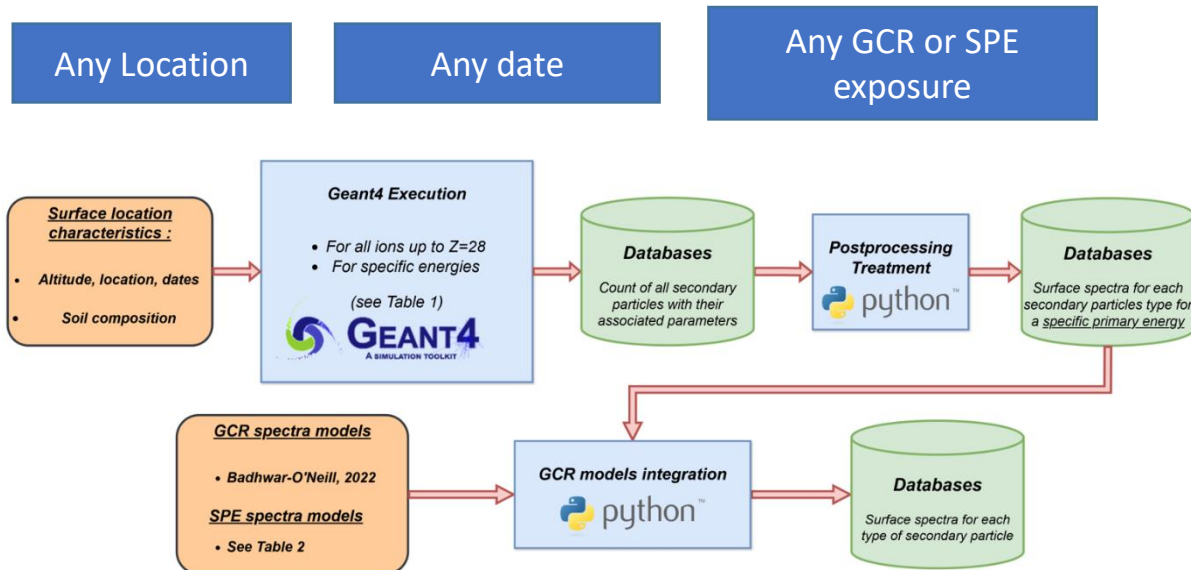
## Main objective :

Reproduce surface flux (including albedo)  
with MC simulation for any local topography  
with special focus for albedo neutrons



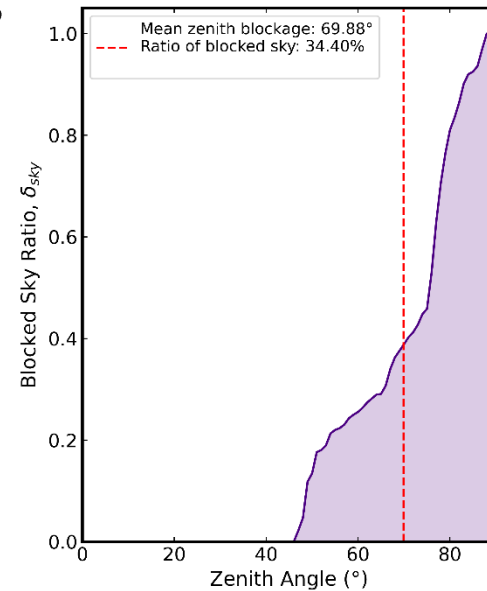
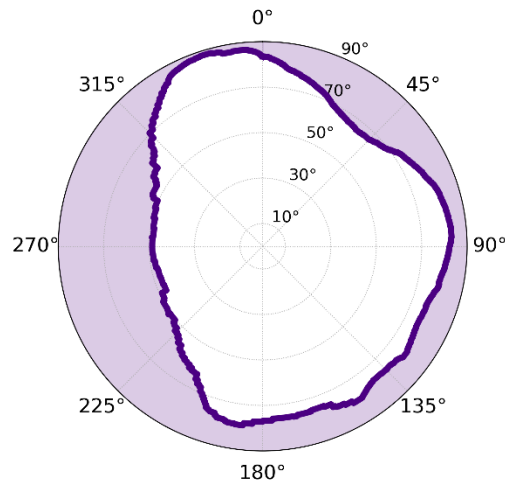
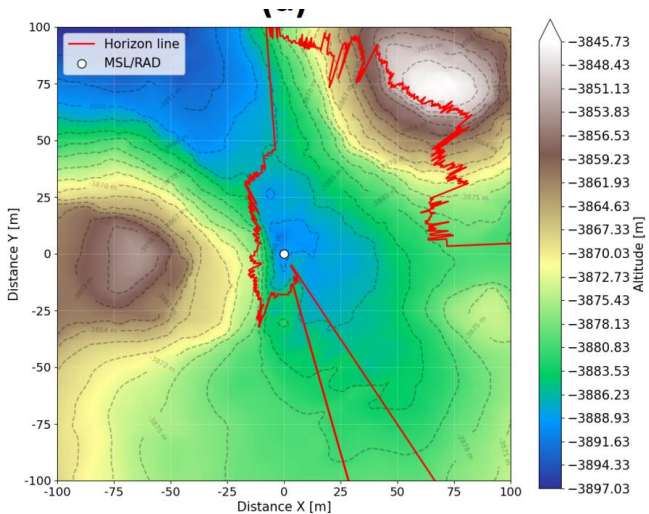
# ARAMIS Environnement Model

- **Radiation Assessment Detector (RAD)**, on board Curiosity rover, provides to date the only measurements of flux and dose from the Martian surface
- **Atmospheric RAdiation Model for Ionizing spectra on martian Surface (ARAMIS)**
  - Monte-Carlo simulations with Geant4 (C++) and Python post-treatment
  - Using the *High Performance Computing* (HPC) center from CNES



Charpentier, et al. (2024), ARAMIS: a Martian radiative environment model built from GEANT4 simulations, *J. Space Weather Space Clim.* 14 35 (2024) DOI: 10.1051/swsc/2024032

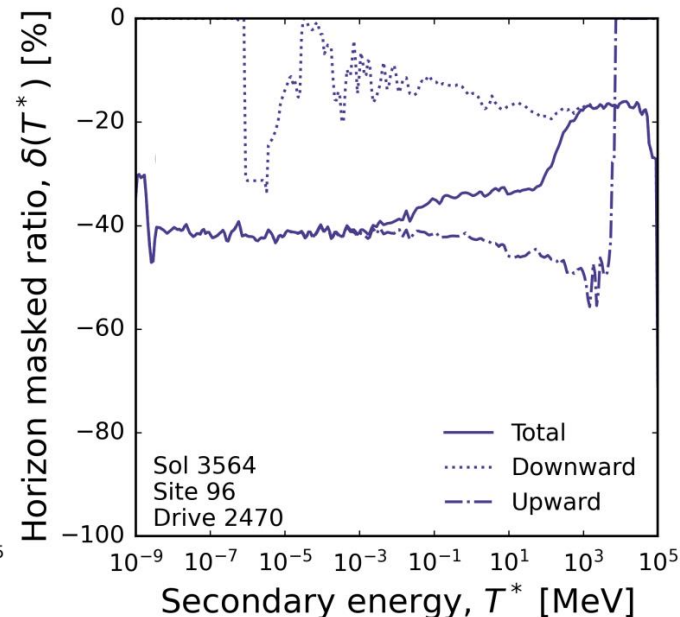
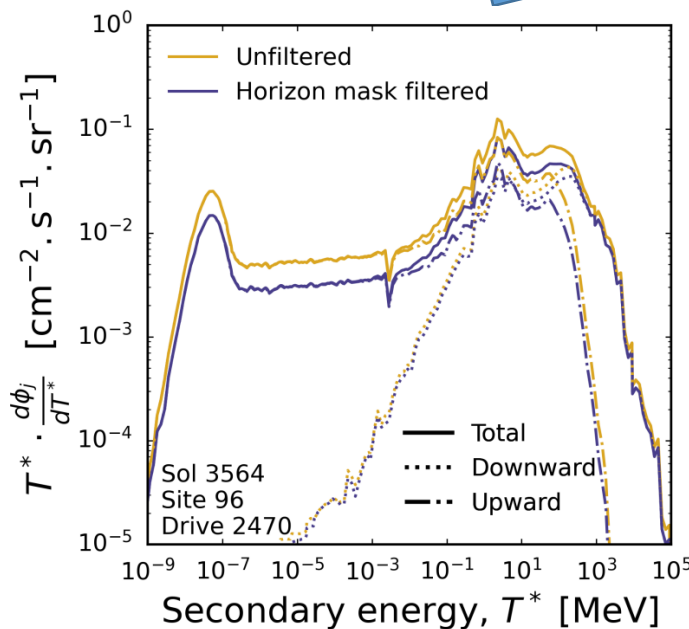
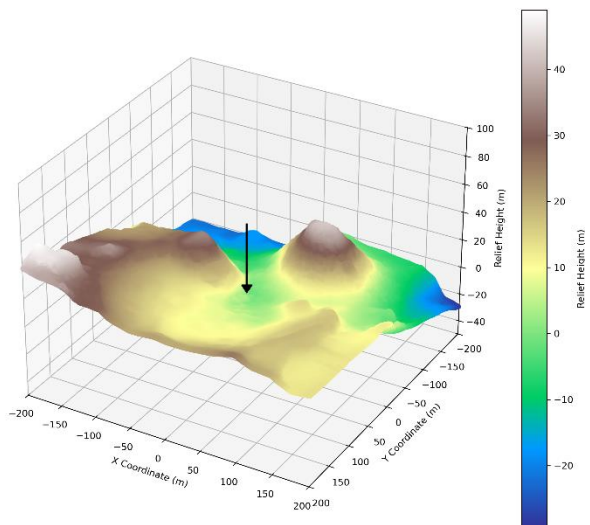
# Natural terrain : results for Paraitepuy Pass



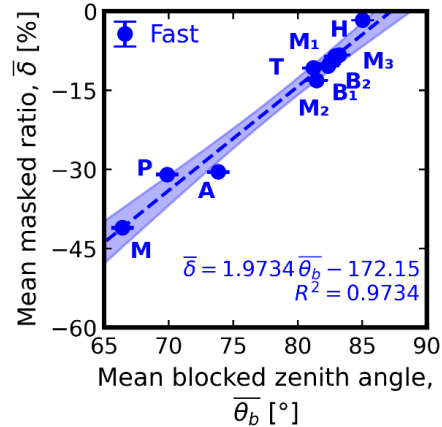
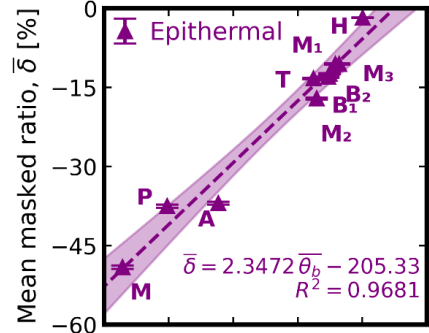
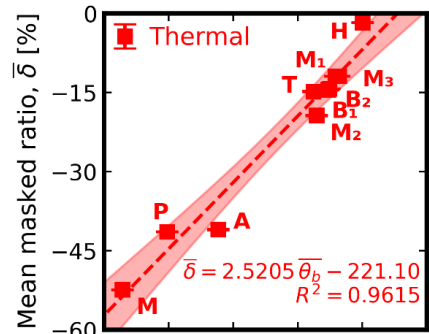
Comparison with flat geometry:

Mean reduction ratio for neutron flux : 33.2% but it depends of the energy

Ratio of blocked solid angle: 34.4%



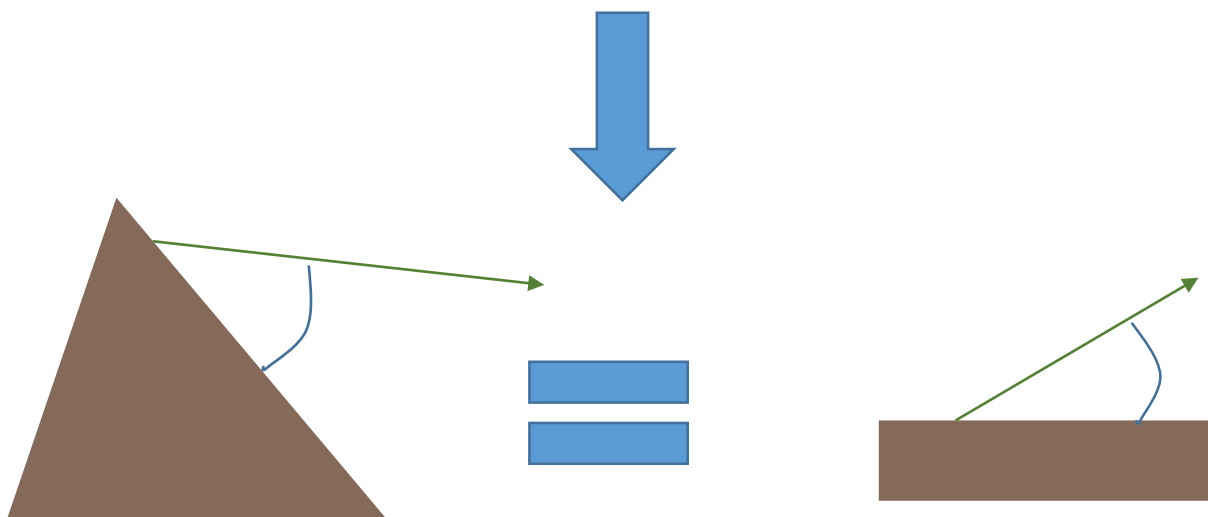
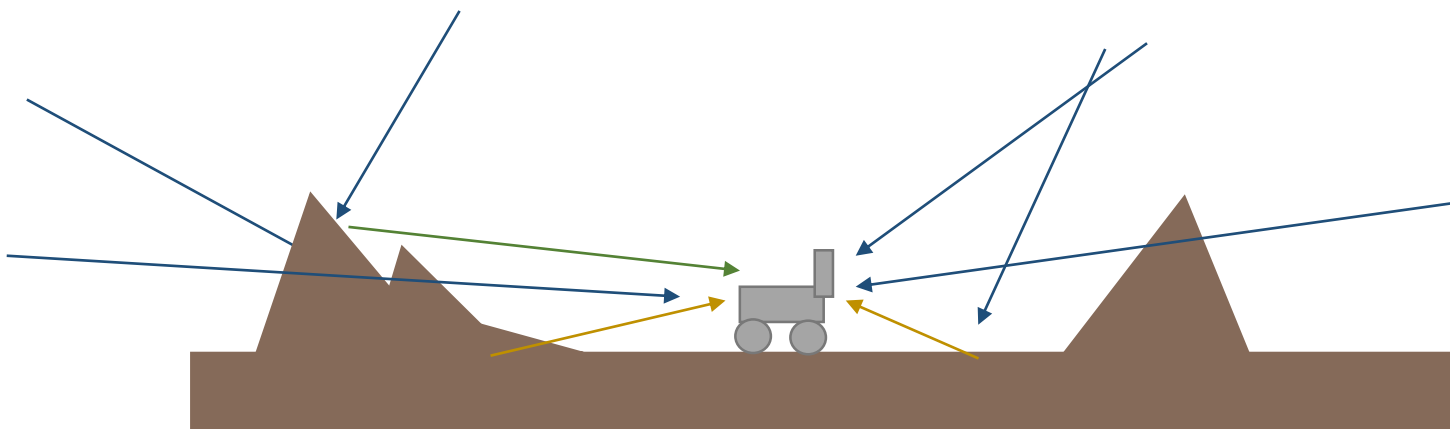
# Natural terrain : results for all the different sites



Location	Mean horizon masked ratio, $\bar{\delta}$ [%]			$\bar{\theta}_b$ [°]	$\delta_{sky}$ [%]
	Downward	Upward	Total		
Hidden Valley	$-1.086 \pm 3.818$	$-1.989 \pm 2.816$	$-1.671 \pm 3.146$	85.01	8.7
Tower Butte	$-4.638 \pm 3.485$	$-15.742 \pm 2.680$	$-11.646 \pm 2.896$	81.21	15.27
Bloodstone Hill - 1	$-4.506 \pm 3.635$	$-15.602 \pm 2.779$	$-11.234 \pm 3.031$	82.34	13.32
Bloodstone Hill - 2	$-4.377 \pm 3.877$	$-14.968 \pm 2.9$	$-10.793 \pm 3.027$	82.45	13.14
Mont Mercou - 1	$-3.735 \pm 3.745$	$-12.6 \pm 3.124$	$-9.180 \pm 3.224$	82.9	12.36
Mont Mercou - 2	$-5.406 \pm 3.473$	$-20.250 \pm 2.724$	$-14.469 \pm 2.812$	81.46	14.85
Mont Mercou - 3	$-3.526 \pm 3.725$	$-12.6 \pm 2.829$	$-9.069 \pm 3.020$	83.21	11.82
Maria Gordon Notch	$-24.995 \pm 2.822$	$-54.132 \pm 1.575$	$-43.744 \pm 1.951$	66.42	40.00
Paraitepuy Pass Approach	$-16.793 \pm 3.326$	$-42.576 \pm 2.062$	$-32.708 \pm 2.291$	73.84	27.83
Paraitepuy Pass	$-16.985 \pm 3.312$	$-43.187 \pm 1.978$	$-33.222 \pm 2.214$	69.88	34.40

- The sky blockage lead to a reduction in thermal, epithermal and fast neutrons fluxes
- A linear regression for the different reduction enabled to find a reduction of 2.52 %/°, 2.35 %/° and 1.97 %/° in thermal, epithermal and fast neutrons flux.

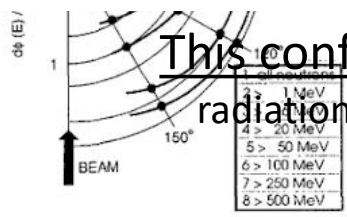
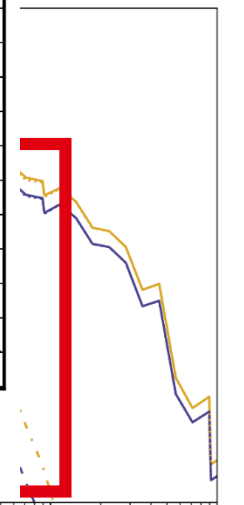
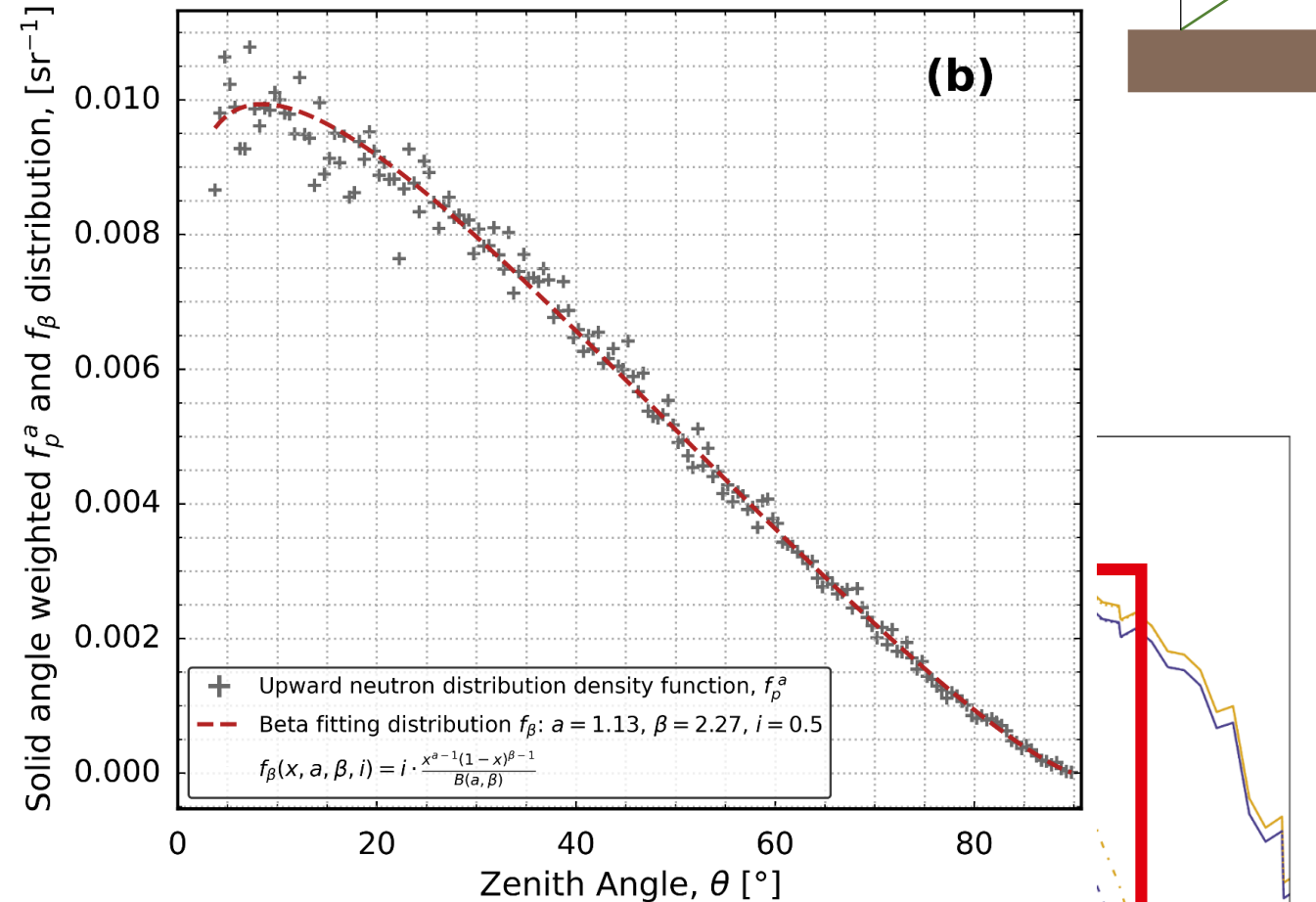
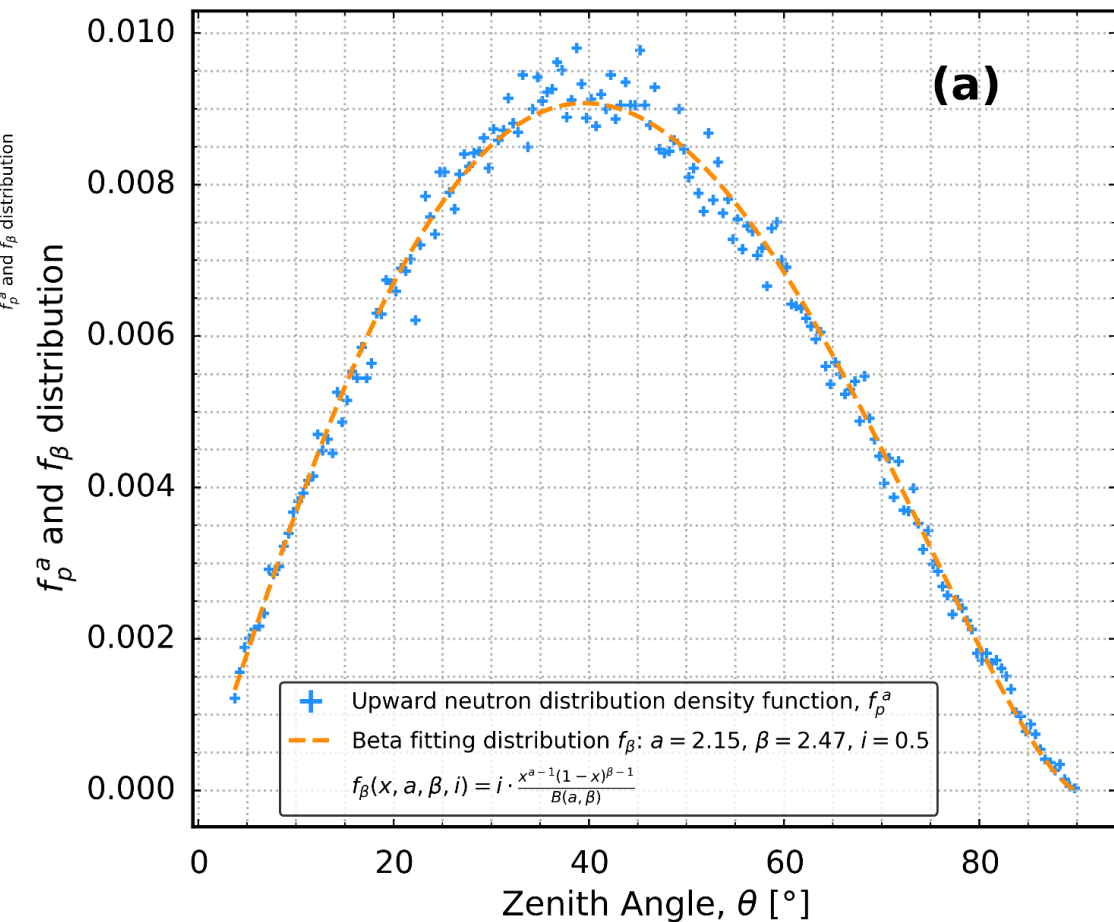
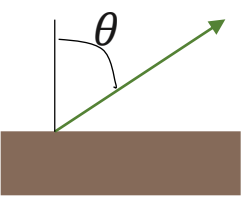
# Natural terrain : Albedo Generation correction factor



HYPOTHESIS:

No interaction between the albedo generated and the atmosphere

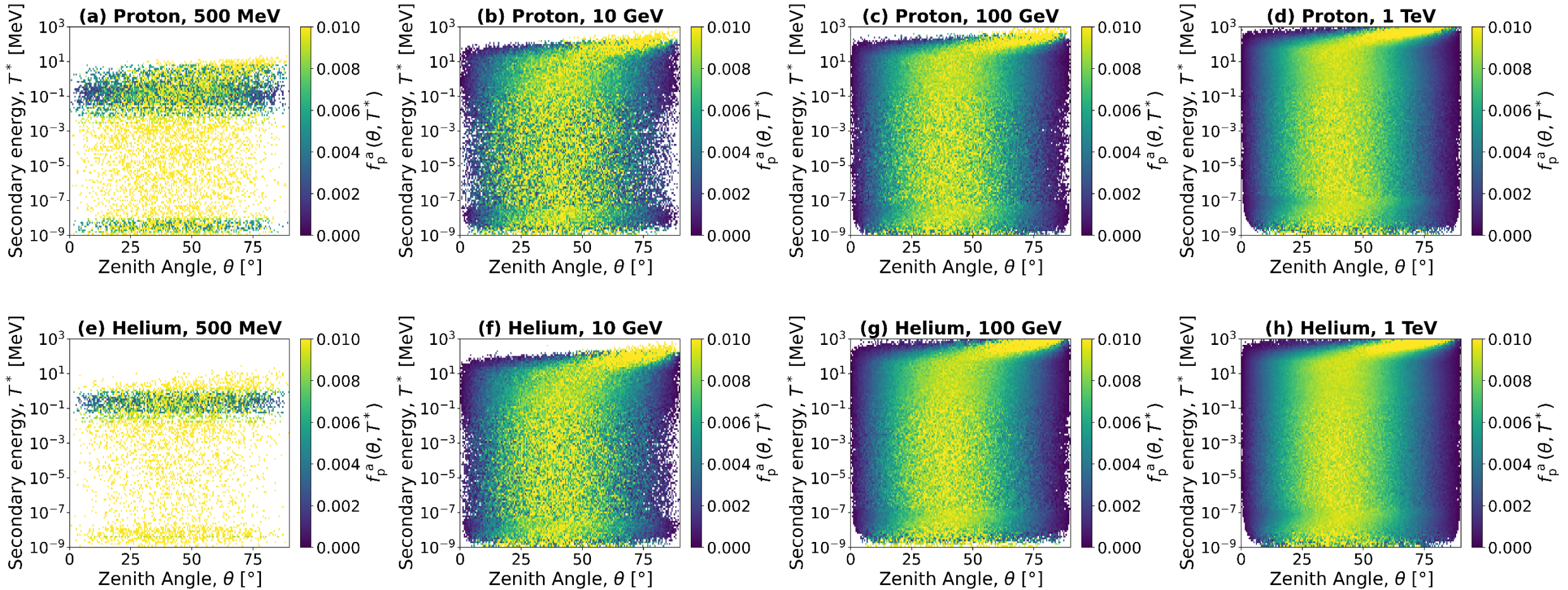
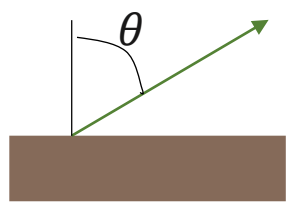
# Natural terrain : Albedo directionality on MC results



This confirms results from : Gonçalves, et al. (2022). Validation of dMEREM, the detailed mars energetic radiation environment model, with RAD data from the surface of Mars. *Frontiers in Astronomy and Space Sciences*, 9, 833144

Low energy : wide scattering angle      High energy : small scattering angle

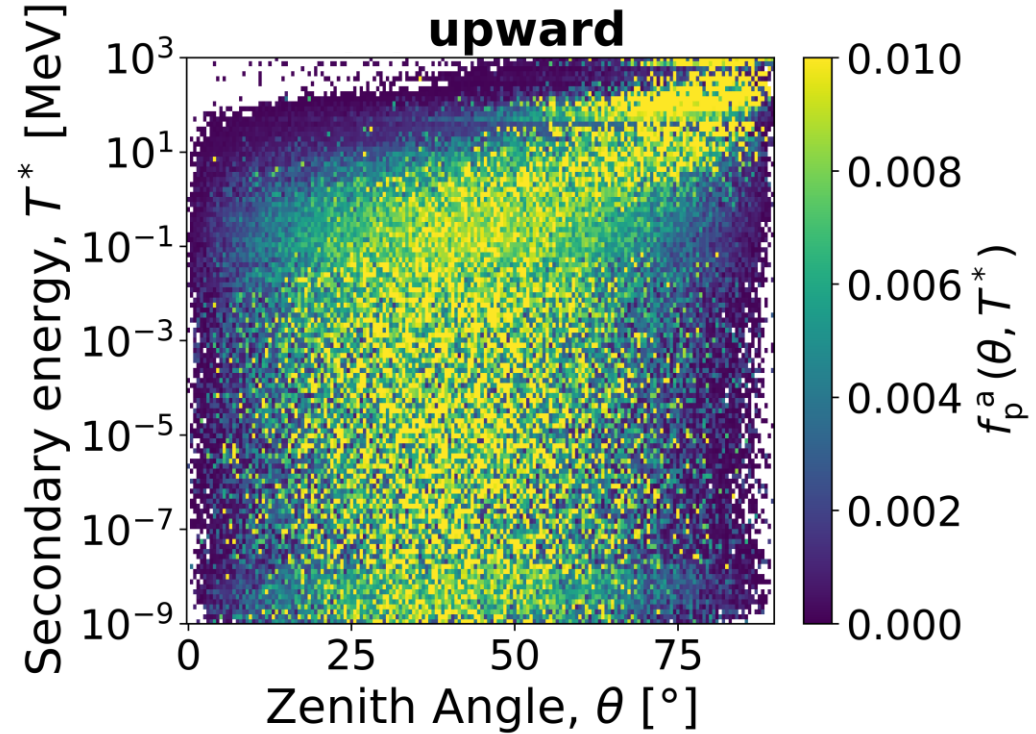
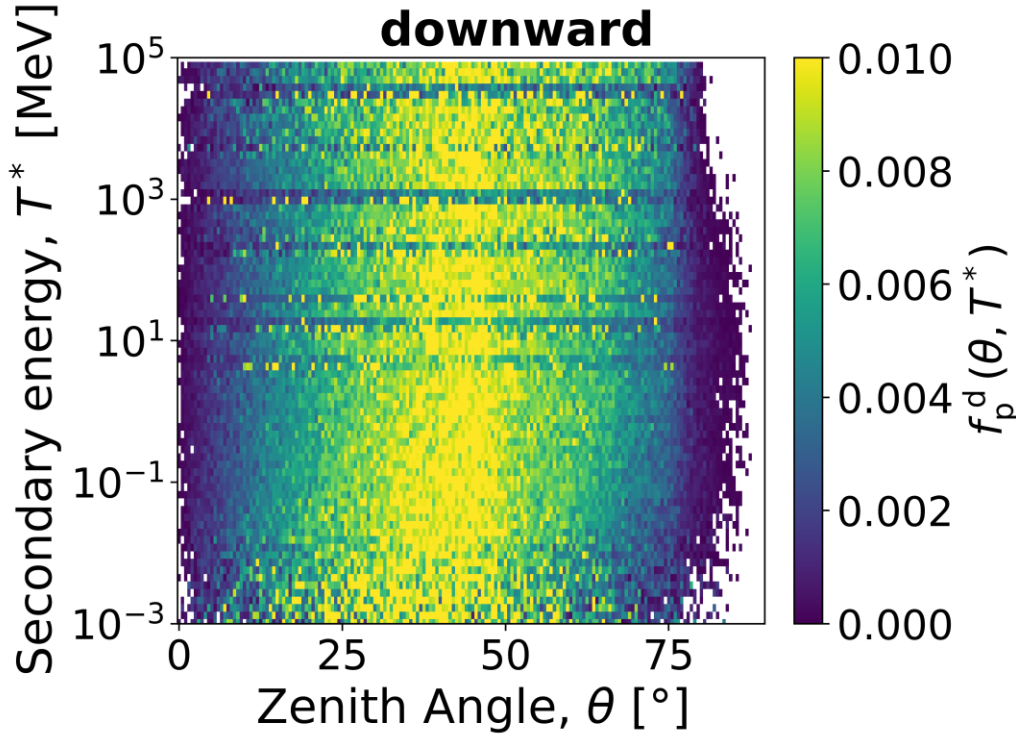
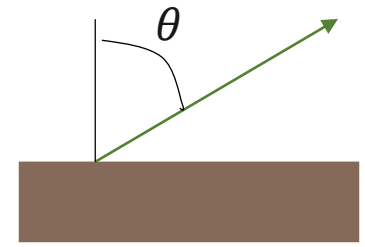
# Natural terrain : **Neutron albedo** directionality on MC results Dependent on **PRIMARY** and **SECONDARY ENERGY**



For different primary energies : 100 MeV, 500 MeV, 1 GeV, 5 GeV, 10 GeV, 50 GeV, 100 GeV, 500 GeV, 1 TeV

After 100 MeV, shift toward high  $\theta$

# Natural terrain : **Albedo** directionality on MC results Convolution with GCR spectra to get the distribution corresponding to sol 3564 (Paraitepuy pass passage)

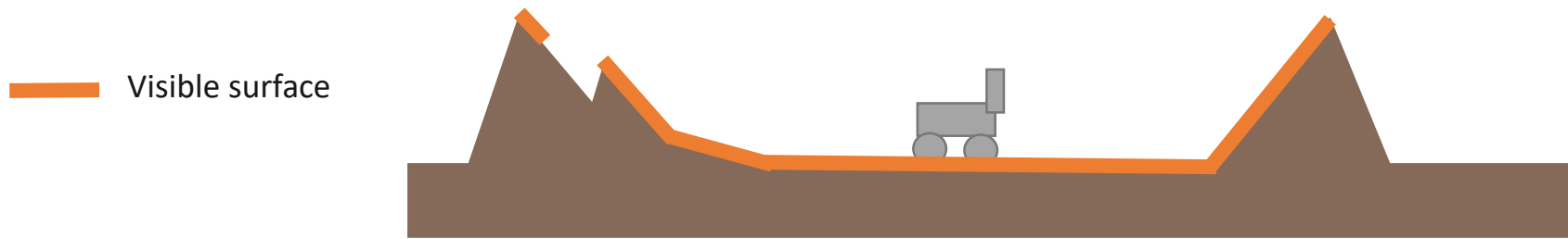


$$f_p^d(\theta, T^*, \varphi) = \frac{N_{flat}^{downward}(\theta, T^*, \varphi)}{\int_{\theta} N_{flat}^{downward}(\theta, T^*, \varphi) d\theta}$$

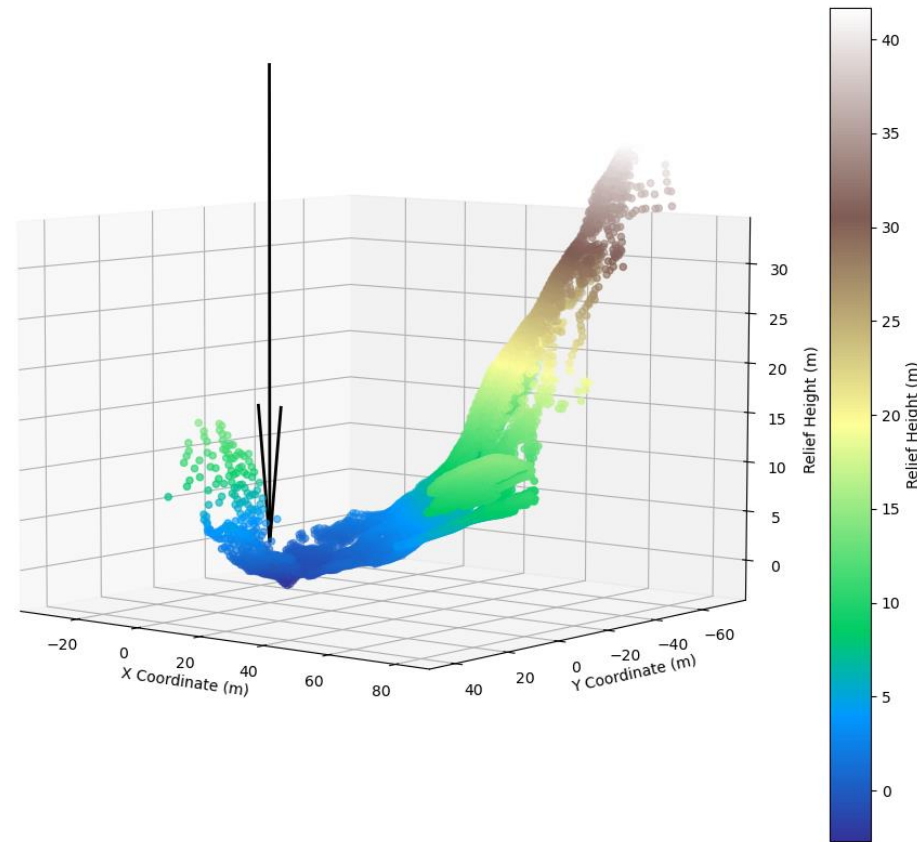
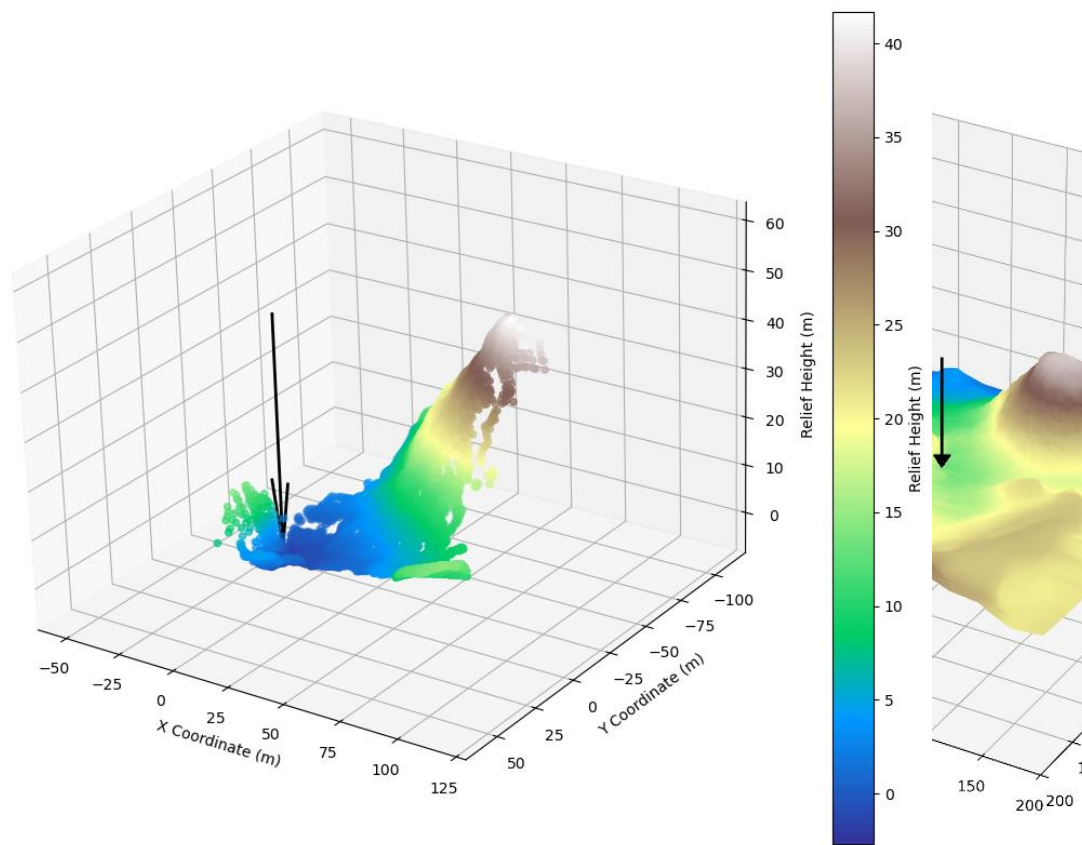
$$f_p^a(\theta, T^*, \varphi) = \frac{N_{flat}^{albedo}(\theta, T^*, \varphi)}{\int_{\theta} N_{flat}^{albedo}(\theta, T^*, \varphi) d\theta}$$

The downward neutron distribution is not taken into account in the further modeling

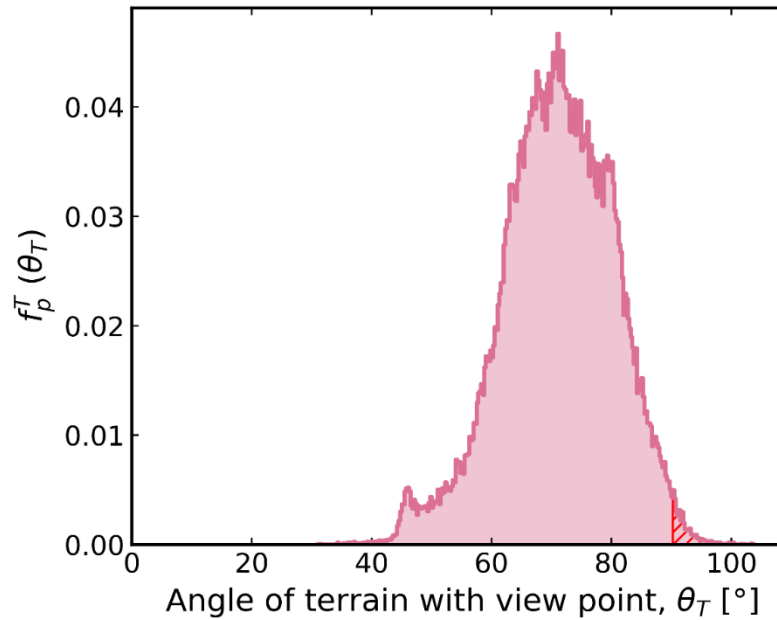
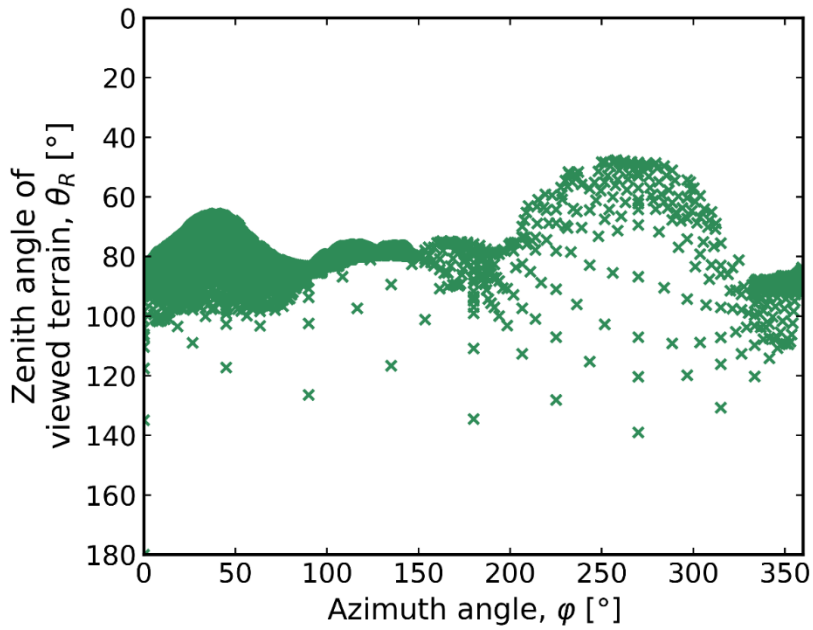
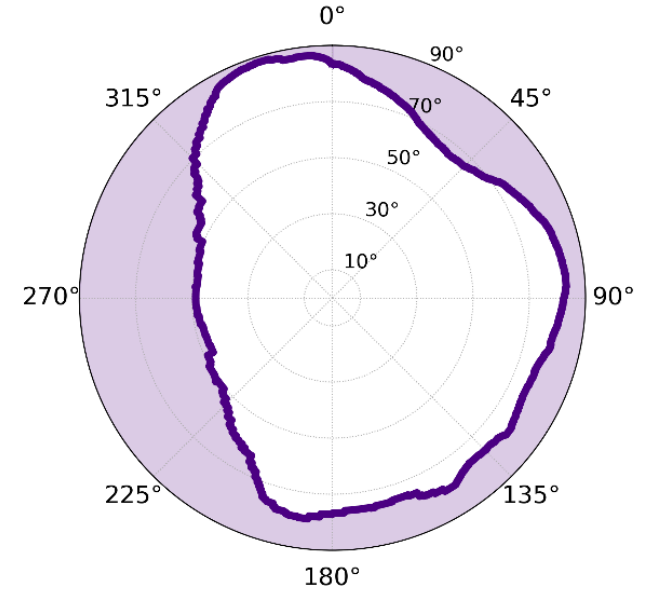
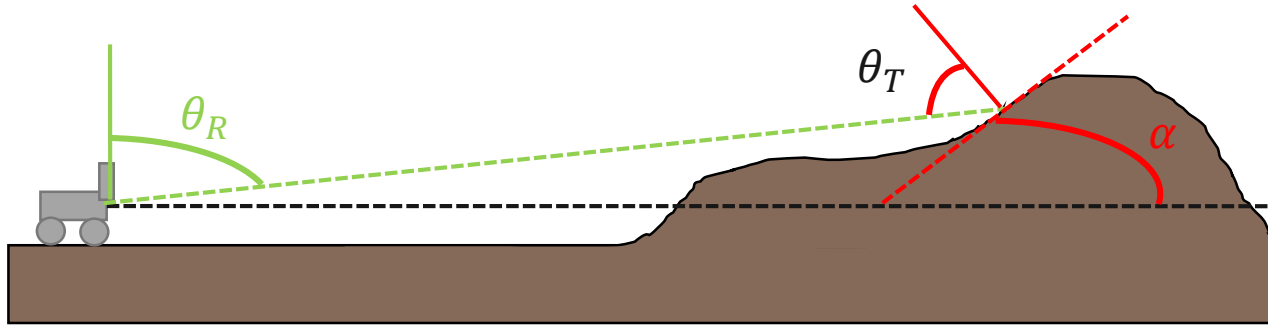
# Natural terrain : Albedo reconstruction with surface viewed



Visibility Map :



# Natural terrain : Albedo Generation correction factor

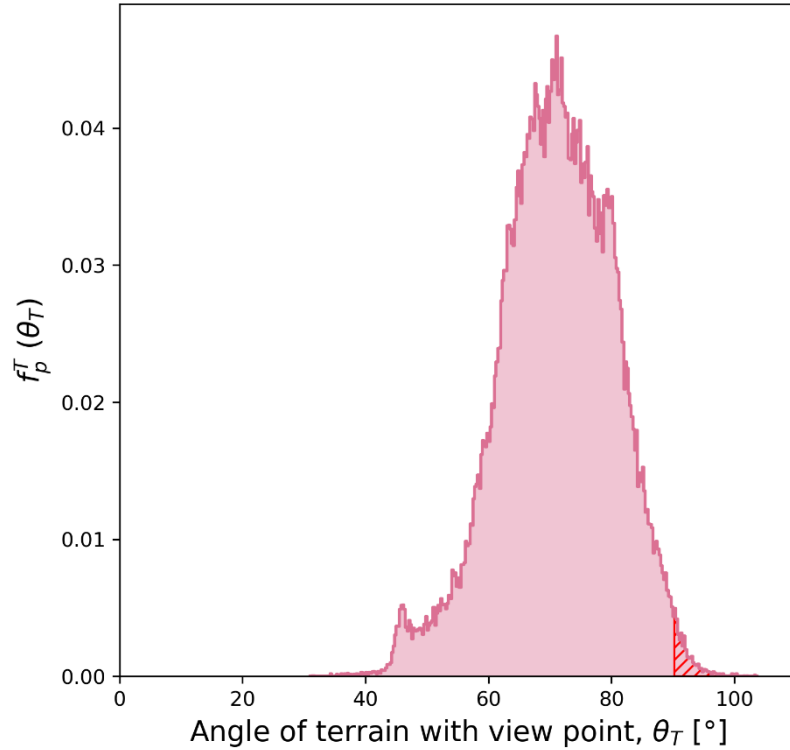


$$f_p^T(\theta_T, \varphi) = \frac{N_{pixels}^{surface\ viewed}(\theta_T, \varphi)}{\int_{\theta} N_{pixels}^{surface\ viewed}(\theta_T, \varphi) d\theta}$$

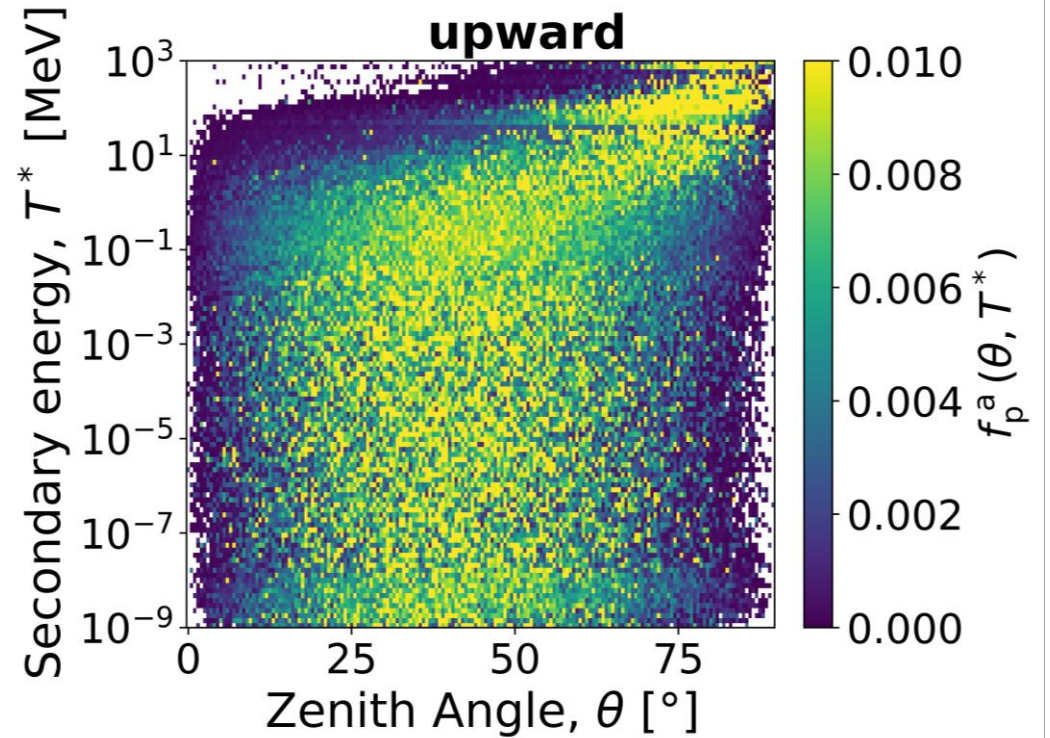
This is only dependent of the local terrain

# Natural terrain : Albedo Generation correction factor

$$f_p^T(\theta, \varphi) = \frac{N_{pixels}^{surface\ viewed}(\theta, \varphi)}{\int_{\theta} N_{pixels}^{surface\ viewed}(\theta, \varphi) d\theta}$$



$$f_p^a(\theta, T^*, \varphi) = \frac{N_{flat}^{albedo}(\theta, T^*, \varphi)}{\int_{\theta} N_{flat}^{albedo}(\theta, T^*, \varphi) d\theta}$$



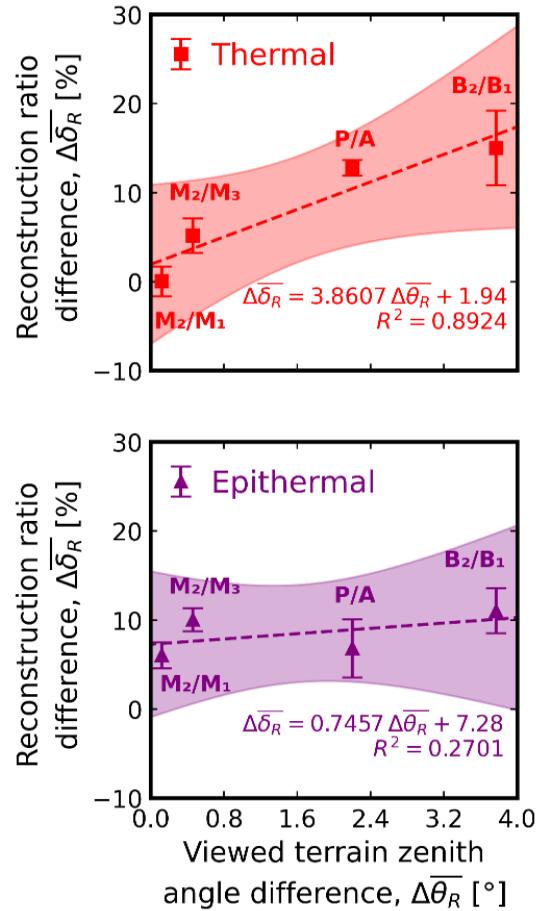
**$\frac{d\Phi}{dT^*}$  Reconstructed Albedo**  
 This is only dependent of the local terrain

**$\frac{d\Phi}{dT^*}$  Masked Albedo**  
 This is dependent of Mars atmospheric parameters and GCR input spectra through correction, but not of the local terrain

$$\beta(\theta, T^*, \varphi) = f_p^T(\theta, \varphi) \cdot f_p^a(\theta, T^*, \varphi)$$



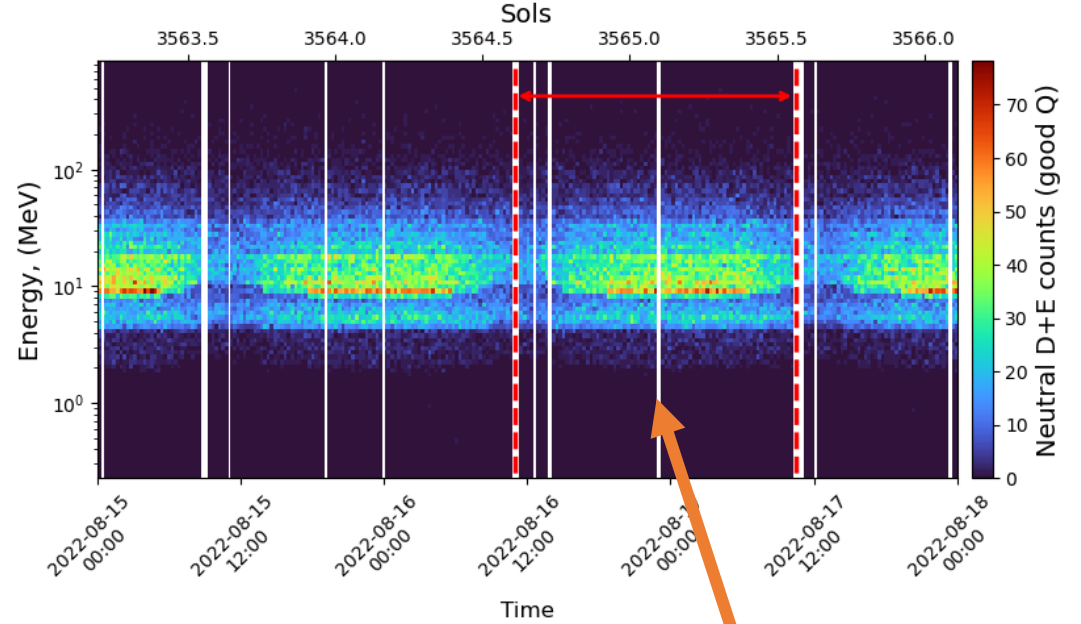
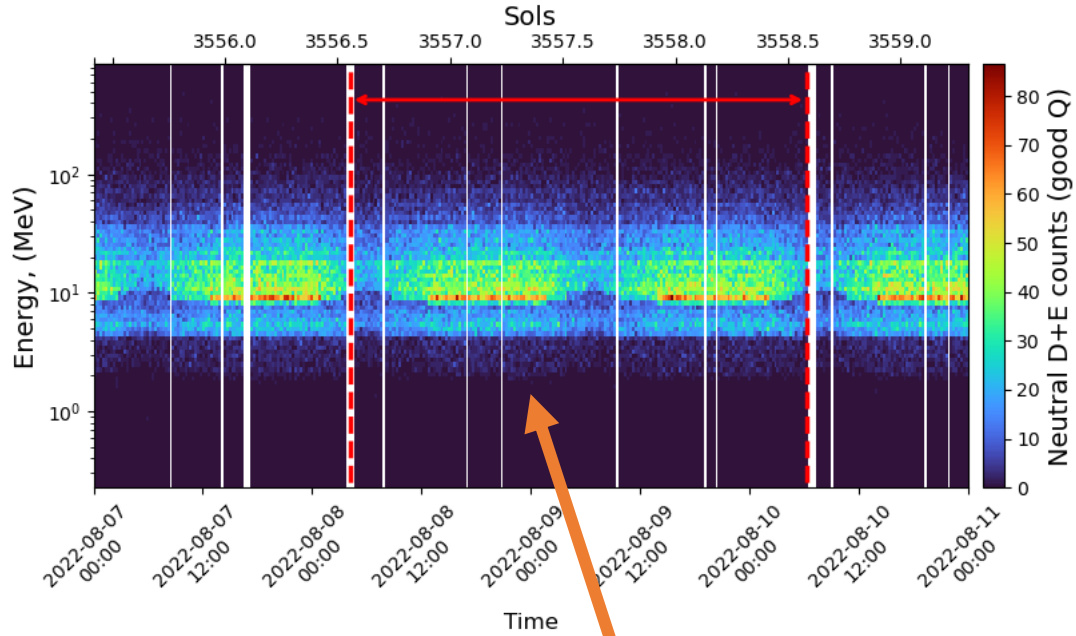
# Natural terrain : reconstruction results for all the different sites



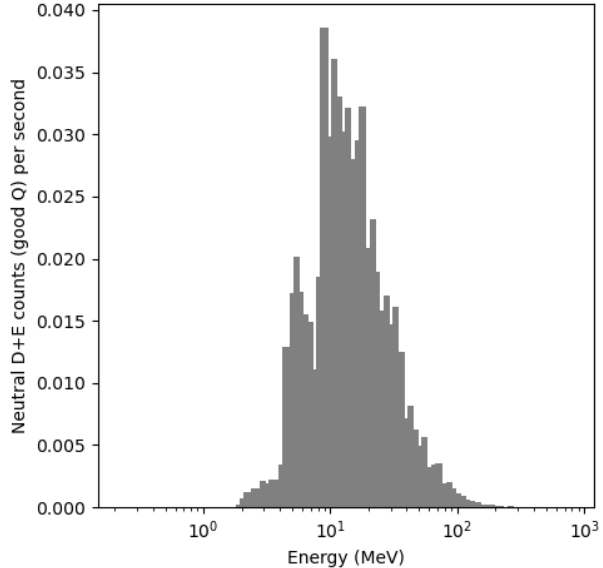
Location	Mean reconstruction ratio, $\bar{\delta}_R$ [%]			$\bar{\theta}_T$ [°]	$\bar{\theta}_R$ [°]	$S_{200}$ [m <sup>2</sup> ]
	Thermal	Epithermal	Fast			
Hidden Valley	-12.119 ± 0.642	-3.466 ± 1.563	-14.825 ± 0.459	83.78	88.03	9340.56
Tower Butte	31.789 ± 3.686	24.681 ± 1.108	9.890 ± 1.316	77.37	95.04	16454.17
Bloodstone Hill - 1	42.338 ± 1.915	35.548 ± 0.978	7.698 ± 0.970	77.9	95.36	27976.5
Bloodstone Hill - 2	57.350 ± 2.271	46.590 ± 1.556	10.256 ± 0.835	78	95.24	27250.17
Mont Mercou - 1	10.524 ± 1.116	7.463 ± 0.732	-3.711 ± 0.583	76.94	84.33	50619.46
Mont Mercou - 2	10.585 ± 0.543	13.515 ± 0.709	-5.464 ± 0.670	76.81	84.79	50855.17
Mont Mercou - 3	5.410 ± 1.404	3.456 ± 0.591	-6.637 ± 0.661	76.59	86.99	47371.7
Maria Gordon Notch	26.418 ± 1.889	17.534 ± 0.677	-2.182 ± 0.910	77.57	93.56	15798.29
Paraitepuy Pass Approach	52.002 ± 0.0	40.668 ± 2.050	10.273 ± 1.086	72.34	82.26	12811.12
Paraitepuy Pass	64.793 ± 0.895	47.510 ± 1.232	-0.743 ± 0.817	71.01	78.49	7071.37

- Unlike the first step; the reconstruction is compared for sites with different points : as the amount of the reconstruction depend of the original filtered flux, point with similar heliospheric and atmospheric conditions must be considered
- For thermal neutrons, the increase is quantified at 3.86 %/° of view zenith angle difference. For epithermal neutron this increase is softer : 0.75%/°.

# Comparison with RAD neutral counts

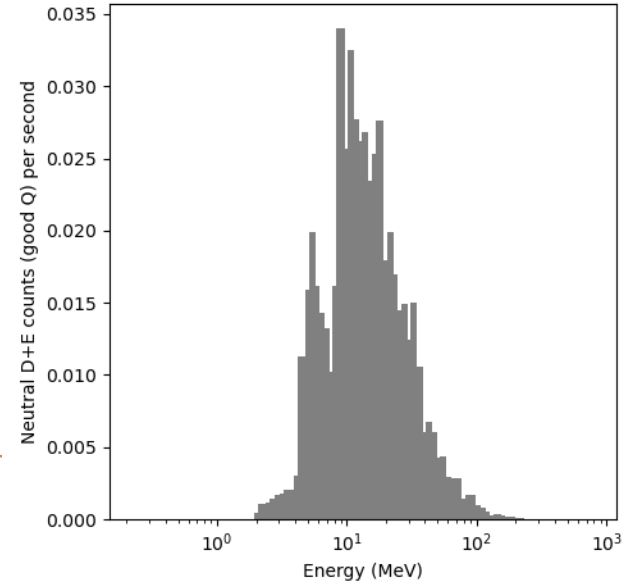


Cumulated Counts while stationed in Paraitepuy Appro



- **MSL – Curiosity parked for ~2 sols in the Approach of paraitepuy pass**
- **Rover Site 96 & Drive 2470**
- **DAN was off**

Cumulated Counts while stationed in Paraitepuy



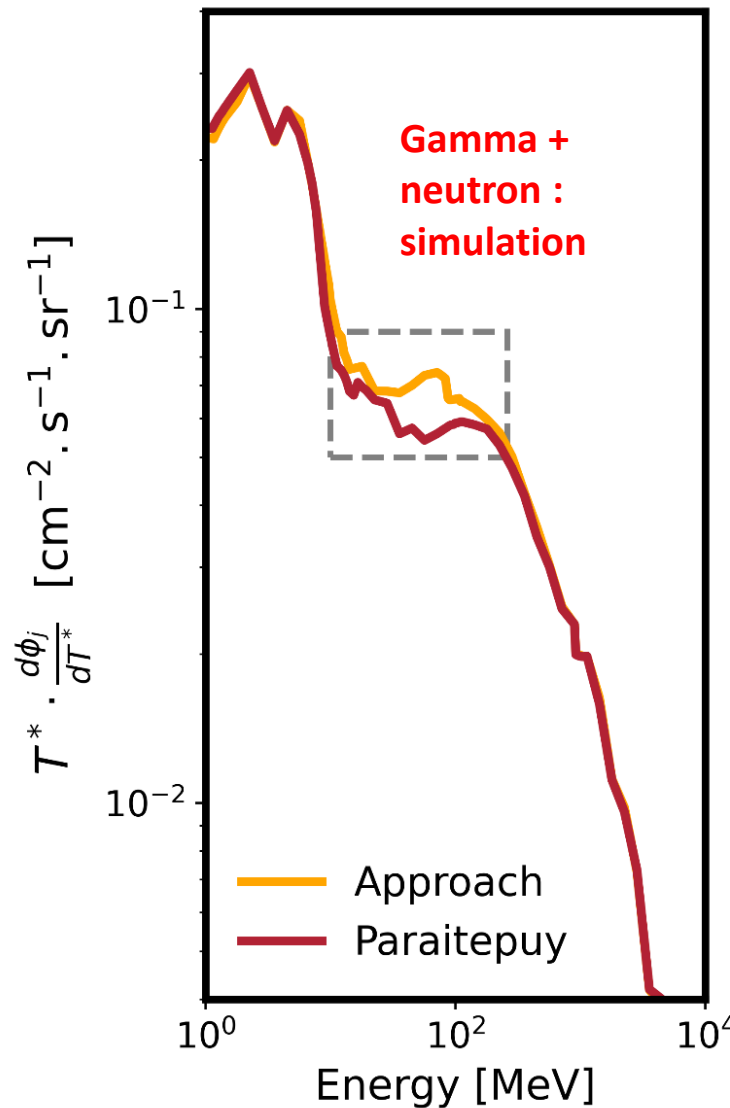
- **MSL – Curiosity parked for ~1 sol in the Approach of paraitepuy pass**
- **Rover Site 96 & Drive 3096**
- **DAN was off**

# Comparison with RAD neutral counts

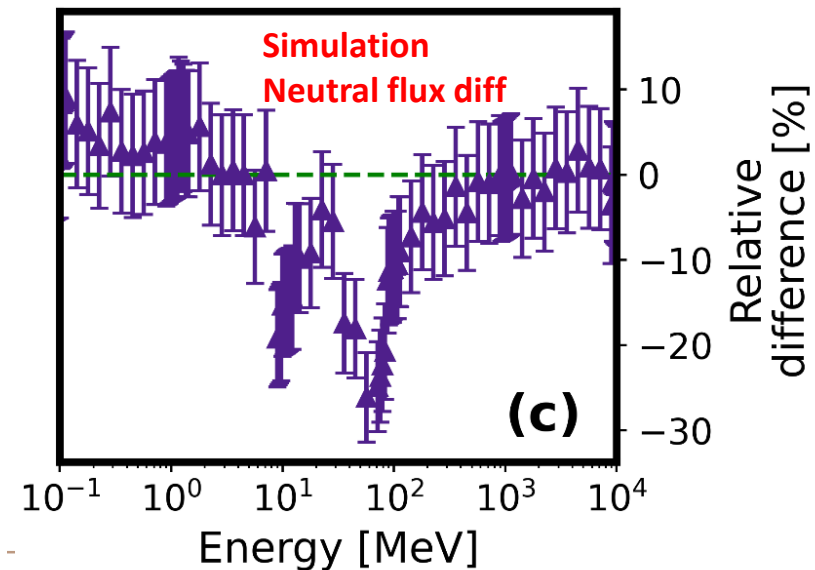
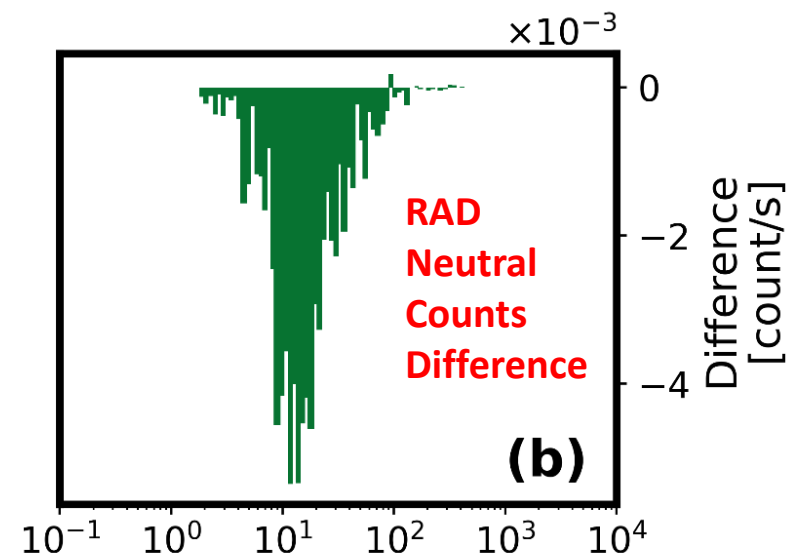
To compare with RAD neutral counts the same methods is used to also reconstruct gamma spectra



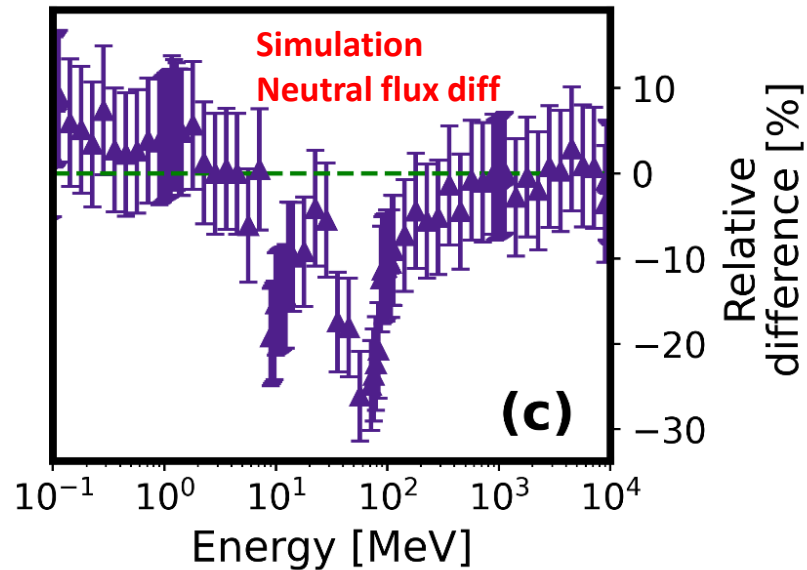
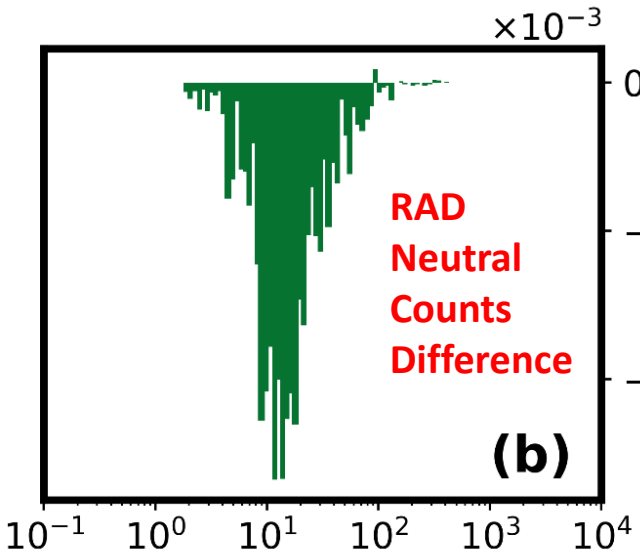
Same procedure for Gamma reconstruction of the flux !



This is not the same quantity !



# Comparison with RAD neutral counts



- Compared with RAD measurements on similar range as for neutron counts
- The reduction between the approach and the pass is on the same order of magnitude between RAD and modeling
- Although tends to have a low estimation of it (on the errors bars)

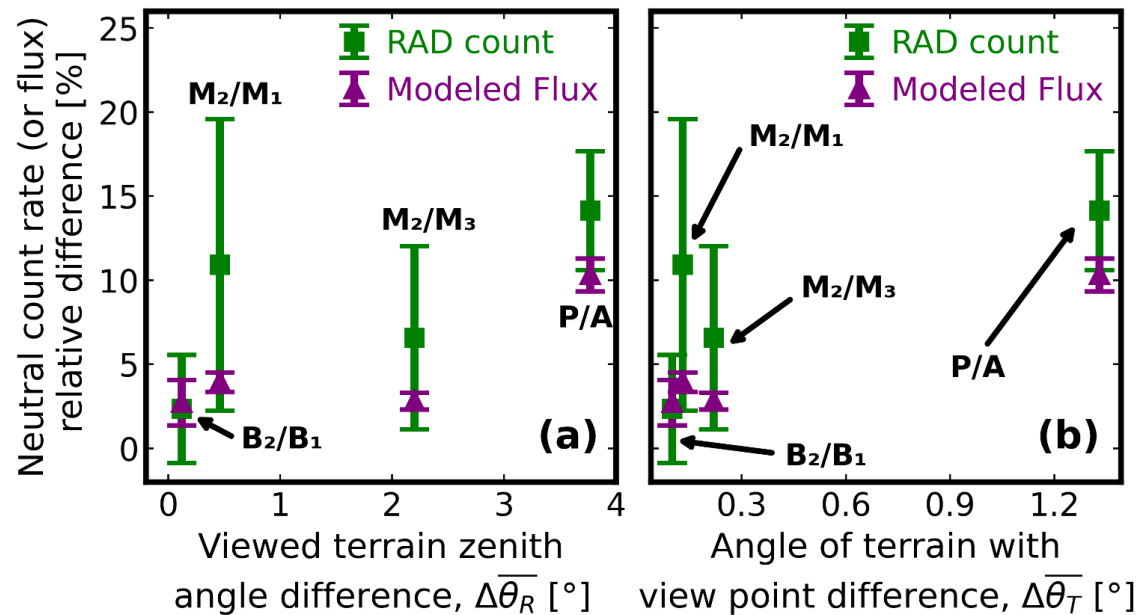
	Neutron	Gamma	Neutron + Gamma	RAD Neutron + Gamma Count
Mean reduction ratio (%)	14.52 ± 1.47 (%)	2.7 ± 1.05 (%)	10.31 ± 0.98 (%)	14.14 ± 3.53 (%)

Ratio on computed reconstructed flux

Ratio on RAD (D+E) counts

# Comparison with RAD neutral counts : other locations

Location	ARAMIS flux variation [%]			RAD count variation [%]
	Neutron	Gamma	Neutron + Gamma	Neutron + Gamma
$B_2/B_1$	$2.72 \pm 0.64$	$9.27 \pm 2.79$	$2.72 \pm 1.35$	$2.34 \pm 3.21$
$M_2/M_1$	$3.79 \pm 0.62$	$3.67 \pm 0.89$	$3.94 \pm 0.58$	$10.92 \pm 8.67$
$M_2/M_3$	$3.97 \pm 0.6$	$2.15 \pm 0.76$	$2.8 \pm 0.5$	$6.58 \pm 5.45$
$P/A$	$14.52 \pm 1.47$	$2.7 \pm 1.05$	$10.31 \pm 0.98$	$14.14 \pm 3.53$



- Even though the RAD error bars are important, a trend appears with a bigger difference (in the fast neutron range) with more obstructed terrain

DOWNLOAD PDF



74

36

## Influence of Mars Topography on Neutral Surface Radiation: Modeling and MSL/RAD Observations

PLANETOLOGY

SOLAR SYSTEM PHYSICS

ALBEDO RADIATION

MARS SCIENCE LABORATORY

RADIATION ENVIRONMENT

SURFACE TOPOGRAPHY



Gabin Charpentier , Jingnan Guo , Salman Khaksarighiri , Rémi Benacquista, Bent Ehresmann , Jean-Christophe Malapert, Robert Ecoffet, Julien Mekki, Alexis Paillet, Sven Loffler, Robert F. Wimmer-Schweingruber , Donald M. Hassler , Cary Zeitlin , Philippe Valet, Yves Gourinat

### Abstract

Since landing in 2012, the Radiation Assessment Detector (RAD) onboard the Curiosity rover has encountered different local landscapes, which have induced variations in the local surface environment. The aim of this study is to include realistic and site-specific local topography for



Charpentier et al., 2025. Influence of Mars Topography on Neutral Surface Radiation: Modeling and MSL/RAD Observations. ESS Open Archive . July 24, 2025 DOI : [10.22541/essoar.175337668.89983018/v1](https://doi.org/10.22541/essoar.175337668.89983018/v1)

# Natural terrain : CONCLUSION

## Key points

- A method to assess surface neutral spectra according to real local topography : can be adapt to any point on the Martian surface
- Thermal neutrons are increasing with local topography for every site encountered. The more surface viewed the more thermal neutrons. This same behaviour has been observed by MSL/DAN.
- On the high energy range the reconstructed flux is lower than for a simulation with flat terrain. It means that the contribution of particle blocked by the landscape is higher than for those 'created' by the terrain.  
Similar observation than with MSL/RAD measurements.

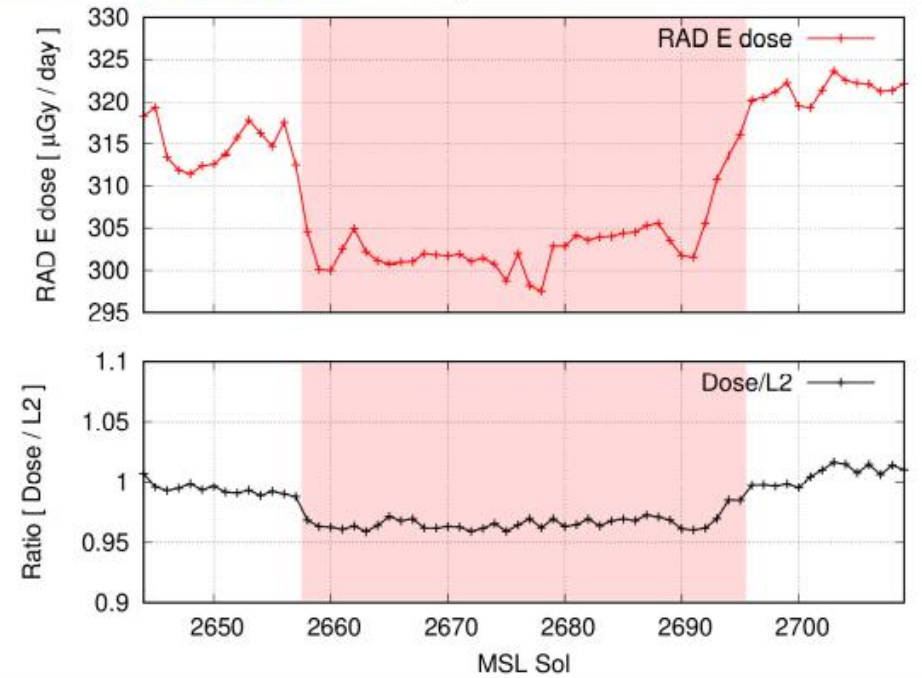
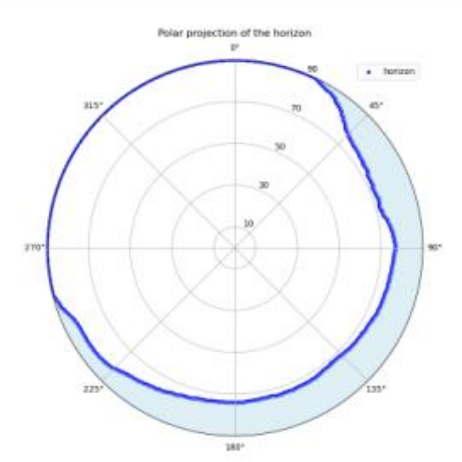
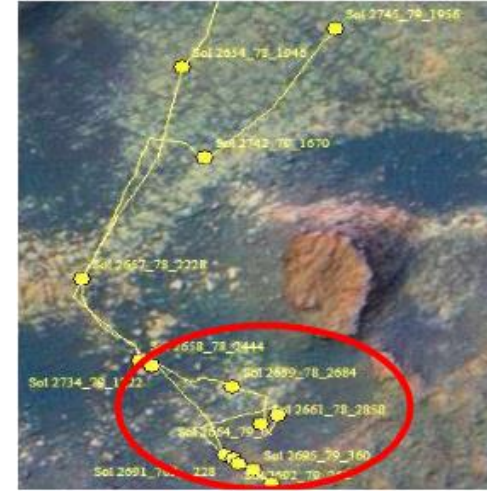
## Future possible advances

- Analysis of possible landing sites to assess the behaviour of neutral particle, and estimate the local dose
  - Integration of this features in local radiative cartographies
    - Similar modeling on the Moon surface



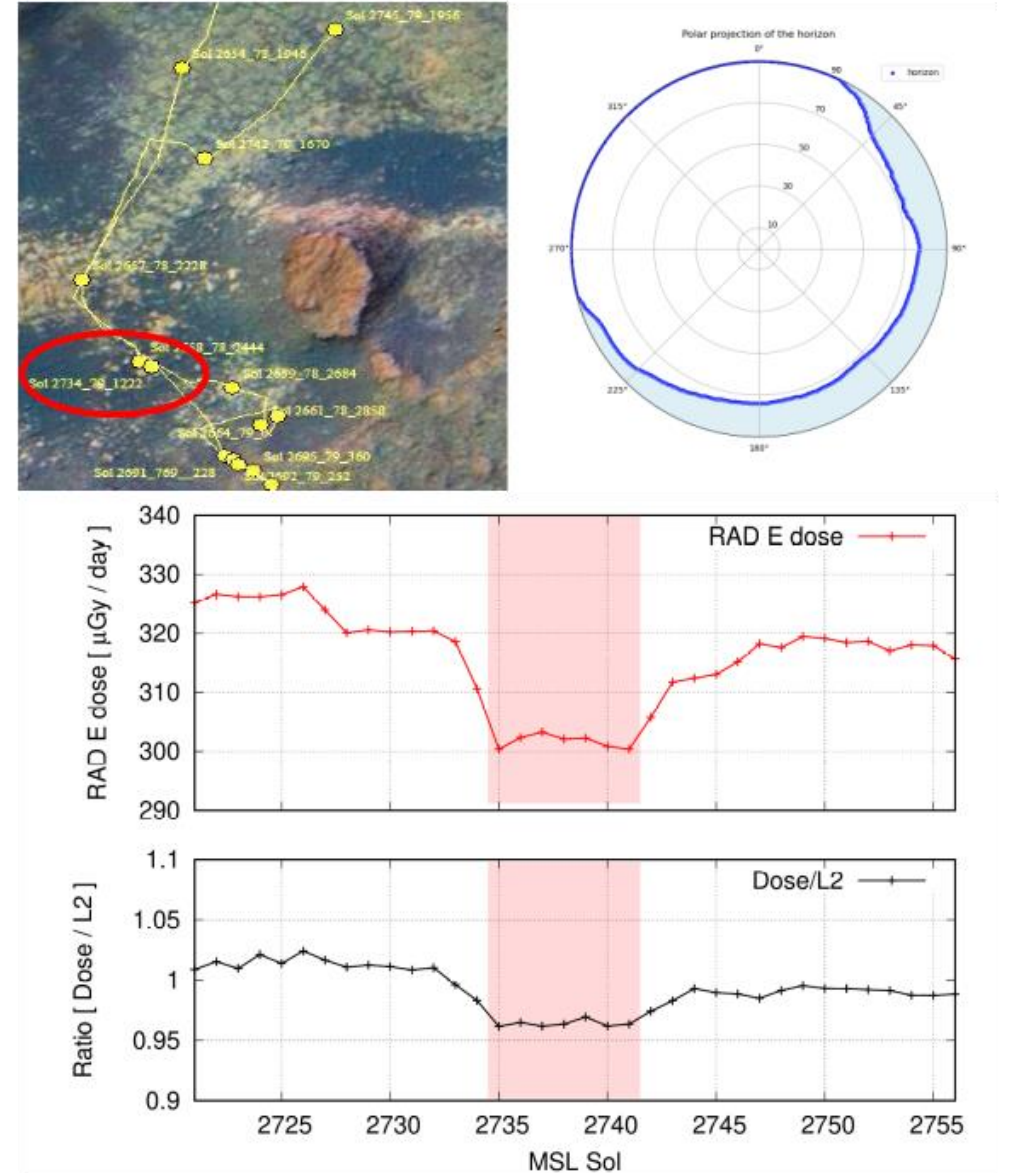
# TOWER BUTTE POSITION 1

- Dose rate measurements (in detector E) are shown in red
- Red shaded area show considered time of shielding
- Bottom panel (black) shows the ratio of dose rate to scaled A\*B counter
- Ratio is ~1 before and after entering the shielded area
- Decrease in radiation: 3.2%
- Average angle of sky obstruction: 8.5°



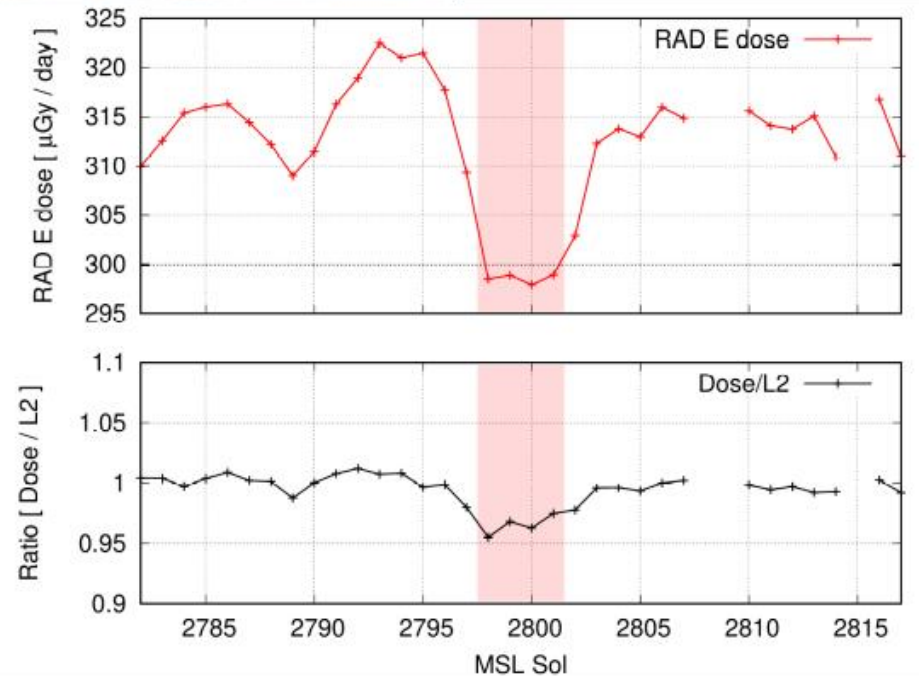
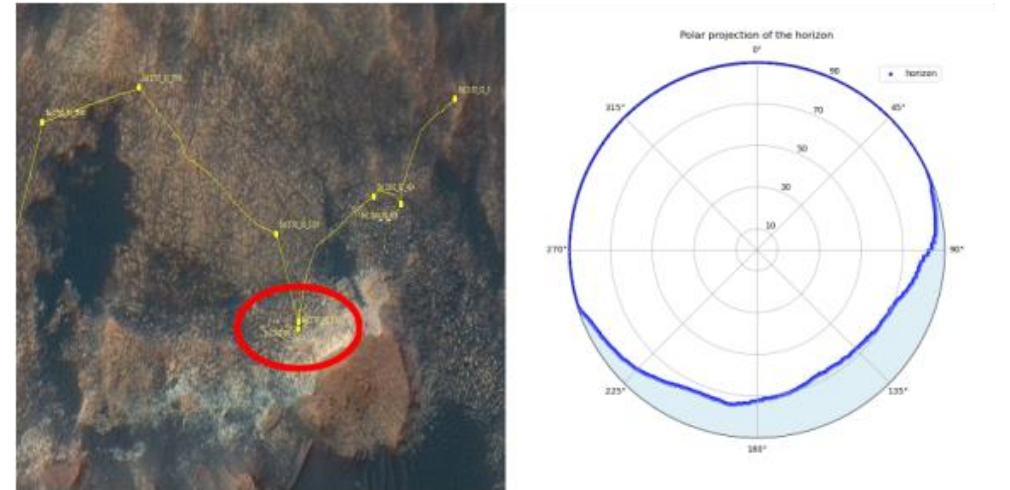
# TOWER BUTTE POSITION 2

- Dose rate measurements (in detector E) are shown in red
- Red shaded area show considered time of shielding
- Bottom panel (black) shows the ratio of dose rate to scaled A\*B counter
- Ratio is ~1 before and after entering the shielded area
- Decrease in radiation: 3.6%
- Average angle of sky obstruction: 8.6°



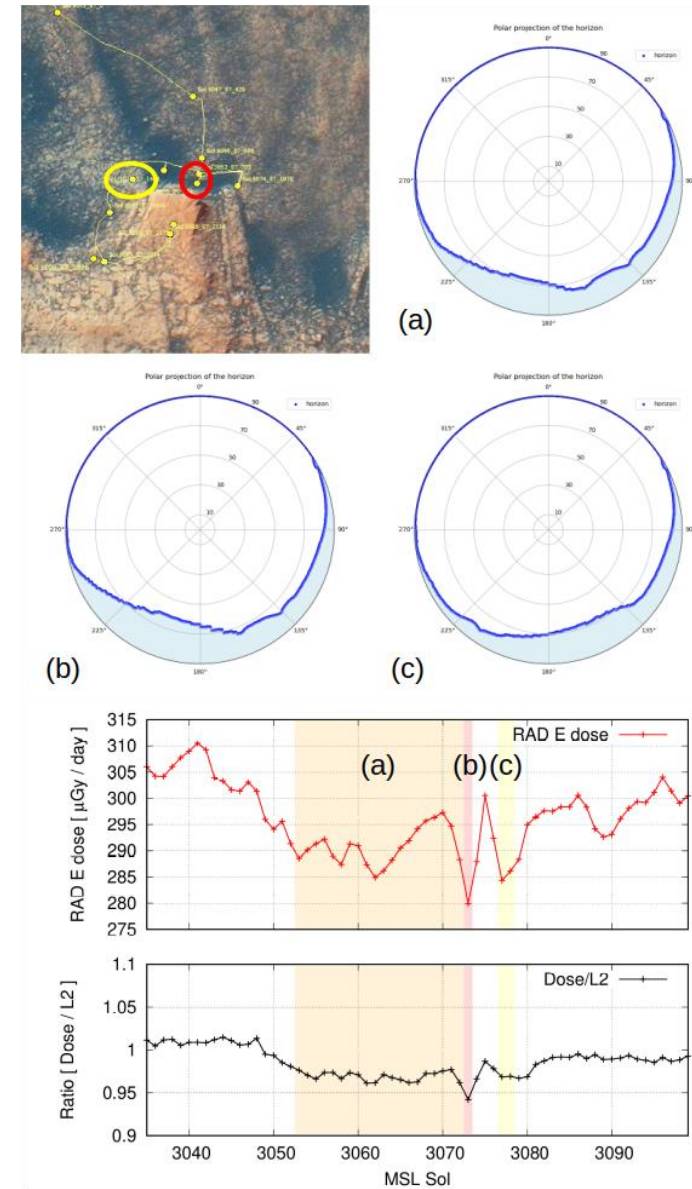
# BLOODSTONE HILL

- Dose rate measurements (in detector E) are shown in red
- Red shaded area show considered time of shielding
- Bottom panel (black) shows the ratio of dose rate to scaled A\*B counter
- Ratio is  $\sim 1$  before and after entering the shielded area
- Decrease in radiation: 3.5%
- Average angle of sky obstruction:  $7.3^\circ$



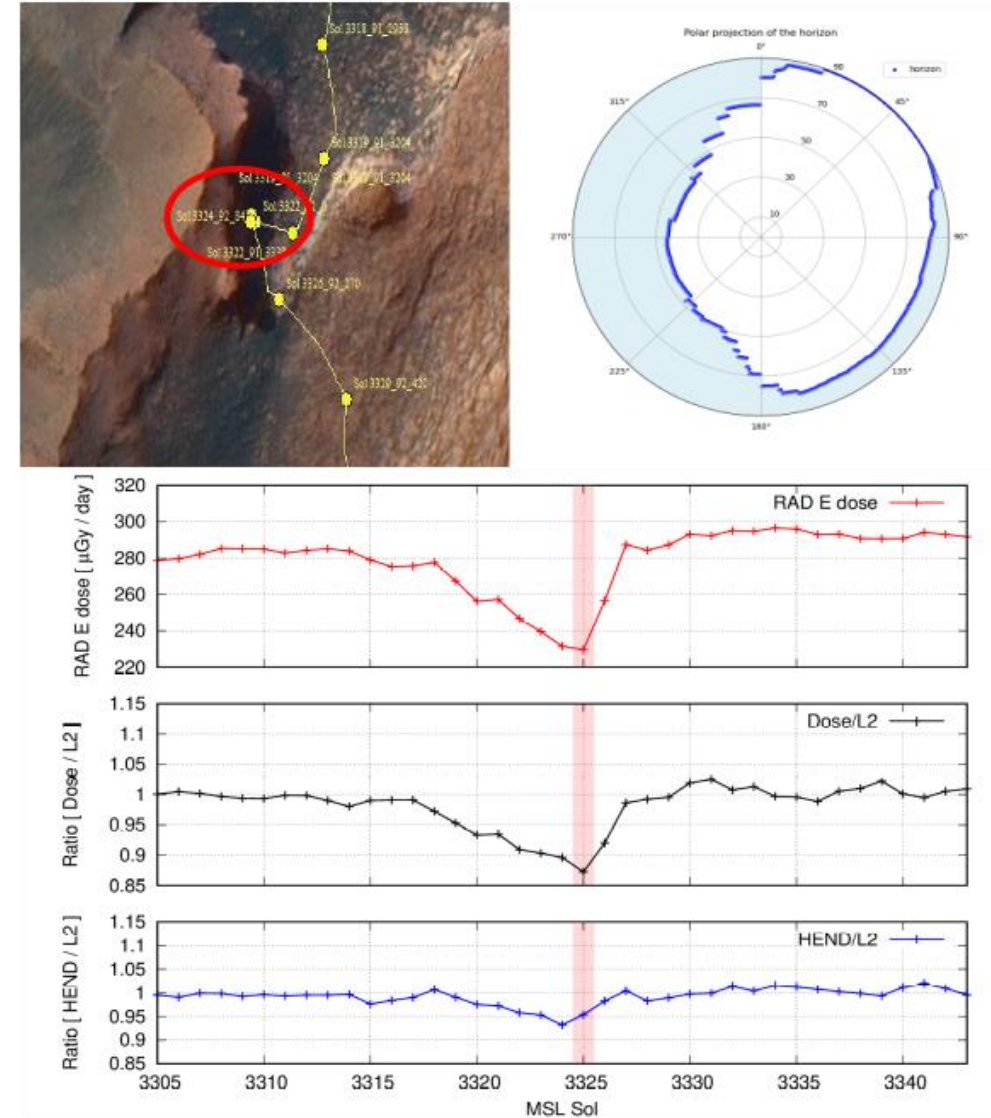
# MT. MERCOU

- Three separate instances where the shielding effect was observed (a,b,c)
- (a) Decrease in radiation: 3.0%
- Average angle of sky obstruction: 6.9°
- (b) Decrease in radiation: 5.8%
- Average angle of sky obstruction: 8.3°
- (c) Decrease in radiation: 3.1%
- Average angle of sky obstruction: 6.5°



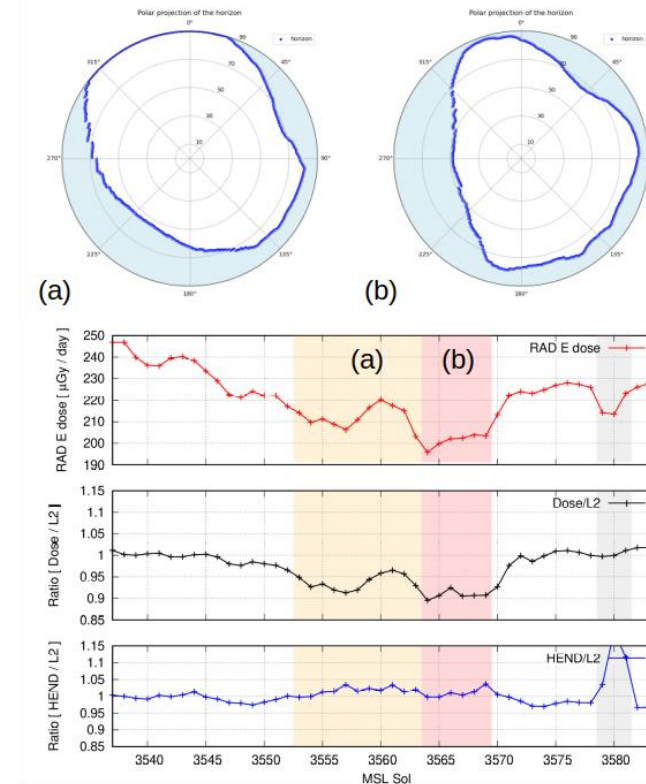
# MARIA GORDON NOTCH

- Decrease in radiation: 12.8%
- Average angle of sky obstruction:  $23.5^\circ$
- Only consider the closest approach at the tightest position when moving through the pass
- Unscaled A\*B counter showed a decrease during the traverse through the pass
- Comparing to orbital HEND GCR proxy counter (blue), we see that there is some shielding effect in the A\*B counter (potential scattering effect)



# PARAITEPUY PASS

- Considered two positions, (a) approaching the pass, (b) traversing the pass
- (a) Decrease in radiation: 6.6%, average angle of sky obstruction:  $16^\circ$
- (b) Decrease in radiation: 9.2%, average angle of sky obstruction:  $20^\circ$
- Dip in dose rate  $\sim$  sol 3580 due to solar effects (HEND shows strong increase in count rate)



# SUMMARY

- Making use of the natural terrain on Mars as radiation shelters provides a great benefit to resource constraints
- RAD has so far observed 11 instances where a significant shielding effect was detectable
- To first order, the decrease in radiation dose linearly scales with the average angle of sky obstruction
- Simplification! Modeling shows that radiation field on the Martian surface becomes more anisotropic the closer to the horizon
- For full modeling the shielding capabilities provided by natural terrain, need to consider terrain in as much detail as possible (DEMs)

<u>Location</u>	<u>MSL Sol</u>	<u>Radiation Decrease</u>	<u>Average Angle of Sky Obstruction</u>
Hidden Valley	707 – 708	1.5% ( $\pm 0.7\%$ )	4.9°
Murray Butte (a)	1456 – 1467	3.8% ( $\pm 0.4\%$ )	8.4°
Tower Butte – Position 1	2658 – 2691	3.2% ( $\pm 1.1\%$ )	8.5°
Tower Butte – Position 2	2735 – 2741	3.6% ( $\pm 1.2\%$ )	8.6°
Bloodstone Hill	2798 – 2801	3.5% ( $\pm 0.6\%$ )	7.3°
Mt. Mercou 1- Drill Position (position a)	3053 – 3072	3.0% ( $\pm 1.0\%$ )	6.9°
Mt. Mercou 2 - Close Approach (position b)	3073	5.8% ( $\pm 1.0\%$ )	8.3°
Mt. Mercou 3 (position c)	3077 – 3078	3.1% ( $\pm 1.0\%$ )	6.5°
Maria Gordon Notch	3324 – 3325	12.8% ( $\pm 1.2\%$ )	23.5°
Paraipetuy Pass Approach	3551 – 3562	6.6% ( $\pm 1.3\%$ )	16°
Paraitepuy Pass	3563 – 3567	9.2% ( $\pm 1.3\%$ )	20°

(a) from Ehresmann et al. (2021)

# THANK YOU FOR YOUR ATTENTION